NASA TECHNICAL TRANSLATION NASA TT F-15,417

DIRECT CALCULATION OF AIRFOILS FROM PRESSURE DISTRIBUTION

R. Eppler

(NASA-TT-F-15417) DIRECT CALCULATION OF AIRFOILS FROM PRESSURE DISTRIBUTION (Scientific Translation Service) 64 p HC $6.25 CSCL 01A

N74-19641

Unclas
G3/01 34376

Translation of "Direkte Berrecnnung von Tragflügelprofilen aus der Druckverteilung," Ingenieur-Archive, Vol. 25, No. 1, 1957, pp. 32-57.

NATIONAL AERONAUTICS AND SPACE ADMINISTRATION
WASHINGTON, D. C. 20546 MARCH 1974

DIRECT CALCULATION OF AIRFOILS FROM PRESSURE DISTRIBUTION

R. Eppler

1. Introduction

/32*

In a recently published paper of the author [1] a method based on conformal mapping was indicated in which airfoil profiles can be calculated from the pressure or velocity distribution. Parameters introduced make it possible to accurately specify the profile thickness and to calculate entire profile series by superposition. However, the method has a disadvantage that the calculated profiles did not exactly correspond to those velocity distributions which were used to start the calculation. Instead, these were afterwards multipled by a factor cos θ, where θ is the inclination angle of the profile which is not known ahead of time. This factor was not very influential at most points on the profile, so that either one has to be satisfied with the resulting velocity distribution or a sufficient correction could be achieved by means of a single correction step. It was only in the vicinity of the nose, where cos θ goes to zero that we could not achieve any agreement between the prescribed velocity and the velocity actually produced. There it was necessary to accept the velocity essentially as determined by the cos factor.

---

*Numbers in the margin indicate pagination of original foreign text.

This advantage is contained in almost all preceding papers.* There is only a paper by M. J. Lighthill [2] which removes this disadvantage, by means of a transformation to the logarithm of the derivative of the complex potential. However, the generality of this method is limited, because it is only possible to deal with especially simple velocity prescriptions which can be evaluated in closed form. In the following we will also use the well-known transition to the logarithm but in the trial solution for the function which is produced, we also split off a singularity, which makes the numerical treatment easier. The prescription of the velocity is then not subjected to any restrictions except for the closure conditions, which must be satisfied, of course. However, these do not represent any difficulties, and can easily be tested and satisfied for the velocity prescriptions.

It again becomes possible to prescribe the velocity for piecewise different angle of attack, as was the case in the preceding paper and was also the case for the paper by Lighthill.** In the present general method, this has particlar advantages. Many advantages of this have been found in the treatment of known problems of profile design. In addition, several new practical problems have been solved in a satisfactory way.

The numerical effort for each profile is somewhat less than in the first method. In particular, in all practical examples, no corrections or iterations are necessary. However, the profile thickness cannot afterwards be specified or changed. The old method should be used when it is necessary to calculate an entire series of profiles with accurately determined thickness, for

*See also the references in Paper [1].

**The paper of Lighthill [2] was not known to me when the preceding paper was published, so that there I erroneously believed the method of prescribing the velocity was new. In the meantime, Professor Dr. Ing. A. Weise, Stuttgart, made me aware of the work of Lighthill.

which the velocity in the vicinity of the wing and nose can go to zero in an uncontrolled way. The new method is applicable if individual profiles are being calculated, for which high accuracy requirements are placed on the velocity distributions along the entire profile, including the nose.

One might have the tendency of not attributing much importance to the vicinity of the nose, as long as no unintentional suction tips are produced there. Therefore, one may prefer the old method. However, it has been found that for the thicker profiles which have a large curvature, the surrounding of the nose in which the cos factor has a large influence does not remain sufficiently small. Here we will also show that a careful treatment of small regions near the nose has greater advantages than generally assumed.

2. The General Trial Solution /33

The present method is also based on the method of conformal mapping. We start with an infinite parallel flow given in the ζ plane by

$$\zeta = \xi + i\eta = re^{i\varphi} \tag{1}$$

around the unit circle (Figure 1). The circulation Γ is determined so that the rear stagnation point is located at $\zeta = 1$. This flow is defined by the complex potential

$$F(\zeta) = \Phi + i\Psi = C\left(e^{-i\alpha}\zeta + e^{i\alpha}\frac{1}{\zeta}\right) - \frac{\Gamma}{2\pi i}\ln\zeta \tag{2}$$

with the circulation

$$\Gamma = 4\pi C \sin\alpha \tag{3}$$

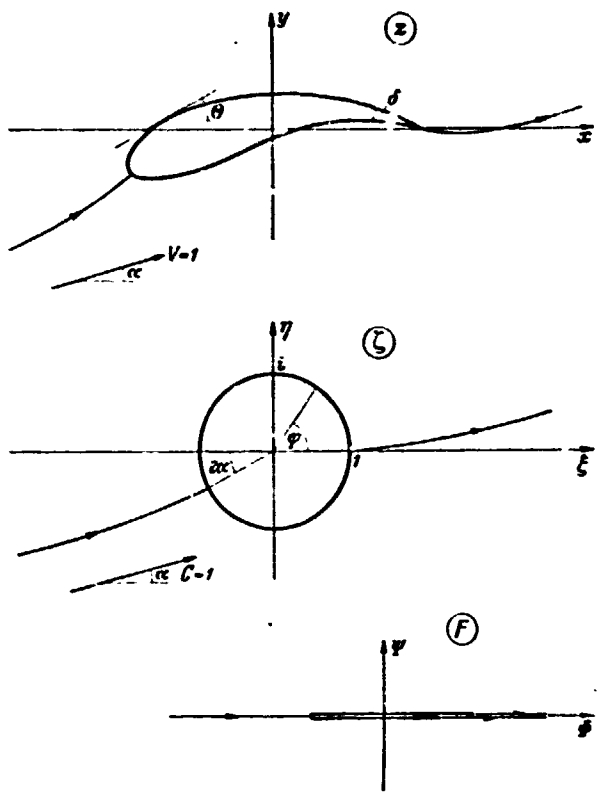

Figure 1. Sketch of the mathematical planes introduced.

We will map this flow onto the z plane by means of a function $z(\zeta)$

$$z = x + iy \tag{4}$$

If the image is also to be an infinite parallel flow with an angle of attack α around an arbitrary profile, then $z(\zeta)$ must map the exterior of the ζ circle onto the exterior of the profile in a conformal manner. $\zeta = 1$ must become the trailing edge of the profile, if a parallel flow is to occur there. At the same time we must have

$$z(\infty) = \infty, \qquad \left(\frac{dz}{d\zeta}\right)_{\infty} = \text{real} \tag{5}$$

Therefore, $z(\zeta)$ can be written in the form

$$z(\zeta) = \beta_1 \zeta + \sum_{\nu=0}^{\infty} \beta_{-\nu} \zeta^{-\nu} \qquad (\beta_1 \neq 0, \text{ real}) \tag{6}$$

with $|\zeta| \geq 1$ as a convergent power series. If the mapping function $z(\zeta)$ is known, then the velocity v in the z plane is given by

$$v = \left|\frac{dF}{dz}\right| = \left|\frac{\frac{dF}{d\zeta}}{\frac{dz}{d\zeta}}\right| \tag{7}$$

and must be calculated as a function of ζ. We will now determine the mapping function $z(\zeta)$ in such a way that along the corresponding profile there will be a prescribed velocity distribution. Usually when the velocity is prescribed, we think of a distribution given over x, and even though strictly speaking it would have to be prescribed over the arc length of the profile. In the preceding paper, we already saw that instead of prescribing $v(x)$, we can specify a function $v(\varphi)$ along the ζ unit circle without any disadvantage. This is because

$$x \approx \frac{l}{2} \cos\varphi \tag{8}$$

(l = length of the profile) is always an approximation of the relationship $x(\varphi)$ for the transition from $v(x)$ to $v(\varphi)$. For a profile of the flat plate, which is produced by $\beta_{-1} = \beta_1, \beta_{-\nu} = 0$ ($\nu = 0, 2, 3, \ldots$), Equation (8) is valid with the equal sign. For adjacent profiles, which wing profiles always are to a certain extent, Equation (8) represents an approximation. Some examples even have much better approximations for $x(\varphi)$ than (8). Should the difference between the initial approximation of a profile and the function $x(\varphi)$ produced for a profile be too large, then the calculated $x(\varphi)$ can be used as the improved approximation /34
for the transition from $v(x)$ to $v(\varphi)$. Then the procedure can start again. This would be quite possible because of the

simplicity of the numerical calculations to be described later on. In all practical calculations up to the present, this improvement was found to be superfluous.

The task of finding a profile for a prescribed $v(\varphi)$ was solved in preceding papers of the author and other papers by introducing a trial solution for the function $z(\zeta)$. In this way, an inconvenient square root was introduced in the equation for the variable $|dz/d\zeta|$ required in (7). In order to avoid this, we will not introduce $z(\zeta)$, but instead according to Lighthill [2]

$$\ln \frac{dz}{dF} = \ln \frac{dz}{d\zeta} - \ln \frac{dF}{d\zeta}. \tag{9}$$

If we introduce the velocity vector of the z plane according to

$$\mathfrak{v} = v e^{i\Theta} \tag{10}$$

then as is well known,

$$\frac{dF}{dz} = \bar{\mathfrak{v}} = v e^{-i\Theta}, \tag{11}$$

and therefore, according to (9),

$$\ln \frac{dz}{dF} = -\ln v + i\Theta \tag{12}$$

This means that we obtain -ln v directly as a real part. Now the function ln dz/dF is regular in the exterior of the ζ circle $|\zeta| > 1$. It can be calculated if its real part is known at the edge [3], that is, if the velocity $v(\varphi)$ is known. If ln dz/dF is known, then according to (9) and (2), $dz/d\zeta$ is specified, and $z(\zeta)$ can be found by integration.

This means we must find a trial solution for ln dz/dF, in which it is possible to calculate the function ln dz/dF from its real part along the edge -ln $v(e^{i\varphi})$ in a simple way. In this trial solution, in contrast to Lighthill [2], we will consider the singularities which occur on the edge $|\zeta| = 1$. They are due in part to the zeros of $dF/d\zeta$, which correspond to the stagnation points of the circle, and according to the equation which follows from (2) and (3),

$$\frac{dF}{d\zeta} = -e^{i\alpha} C\left(\frac{1}{\zeta} - 1\right)\left(\frac{1}{\zeta} + e^{-2i\alpha}\right) \tag{13}$$

they lie at $\zeta = 1$ and at $\zeta = -e^{2i\alpha}$. On the other hand, $dz/d\zeta$ has a zero at $\zeta = 1$ (see Figure 1), if the trailing edge of the profile is to be produced at the image of its point. If the flow is to leave the profile with a finite velocity, then dF/dz does not vanish at $\zeta = 1$, which means that the two singularities of $dF/d\zeta$ and $dz/d\zeta$ cancel there in (9). The trailing edge angle of the profile must vanish. A finite trailing edge angle in (9) would have a singularity as a consequence at $\zeta = 1$, which could have easily been overlooked. In the following we will not consider it. Instead, in section 5d) we will show how one obtains complete profile trailing edges which are satisfactory when the trailing edge angle vanishes. According to (9), we will introduce the trial solution

$$\ln \frac{dz}{dF} = -\ln C - \ln\left[e^{i\alpha}\left(\frac{1}{\zeta} + e^{-2i\alpha}\right)\right] + \sum_{m=0}^{\infty} (a_m + i\, b_m)\,\zeta^{-m}. \tag{14}$$

Using a power series which converges over the entire edge $|\zeta| = 1$, which will be required later on, we find for $\zeta = 1$ a finite dz/dF, that is a smooth flow off the profile and zero trailing edge angle. From (14) and by comparison with (9) and (13), we find

$$\ln \frac{dz}{d\zeta} = \ln\left(1 - \frac{1}{\zeta}\right) + \sum_{m=0}^{\infty} (a_m + i\, b_m)\zeta^{-m}. \tag{15}$$

This function has a singularity at $\zeta = 1$, because there, angles are doubled in the transition from ζ to z, but there are none at the front stagnation point. The mapping becomes conformal there and the profile is the image of the circle and has a continuous tangent there.

The function which is a consequence of (15) /35

$$\frac{dz}{d\zeta} = \left(1 - \frac{1}{\zeta}\right) e^{\sum_{m=0}^{\infty} (a_m + i b_m)\zeta^{-m}} \tag{16}$$

must be compatible with (6). It is analytical in $|\zeta| > 1$, just like (6), because this is the case for the series in the exponent. It is also possible to order (16) with respect to decreasing powers of ζ and to compare the result with the derivative of (6). This comparison requires that

$$b_0 = 0, \tag{17}$$

$$a_1 = 1, \tag{18}$$

$$b_1 = 0. \tag{19}$$

The first condition provides that there will be no rotation at infinity, (18) and (19) make the term ζ^{-1} vanish. At the same time, we are sure that a closed profile is produced by the integration of (16). Therefore, we will call (18) and (19) the closure conditions.

We will also provide for unit flow velocity at infinity. According to (14), this requires that

$$V = v(\infty) = C e^{-a_0} = 1, \tag{20}$$

which is obtained by setting

$$C = 1, \tag{21}$$

$$a_0 = 0 \tag{22}$$

Accordingly, the velocity v can always be interchanged with the velocity ratio v/V which occurs in the Bernoulli equation

$$\frac{p - p_\infty}{\frac{\varrho}{2} V^2} = 1 - \left(\frac{v}{V}\right)^2 \tag{23}$$

in the calculation of the pressure p.

The problem formulated states that the free variables a_m, b_m must be determined in such a way that for $\zeta = e^{i\varphi}$, the velocity $v(\varphi)$ calculated according to (14) and (12) have a given variation. For this purpose, we introduce $\zeta = e^{i\varphi}$ in (14) and set

$$P(\varphi) = \sum_{m=0}^{\infty} a_m \cos m\varphi + b_m \sin m\varphi, \tag{24}$$

$$Q(\varphi) = \sum_{m=0}^{\infty} -a_m \sin m\varphi + b_m \cos m\varphi. \tag{25}$$

By separating the real and imaginary parts, we find

$$\left.\begin{aligned} -\ln v(\varphi) + i\,\Theta(\varphi) = -\ln 2 \left|\cos\left(\frac{\varphi}{2} - \alpha\right)\right| + P(\varphi) + i\left[\frac{\varphi}{2} + Q(\varphi) - \{\{\pi\}\}\right], \\ \text{where} \qquad \{\{\pi\}\} = \begin{cases} 0 & (0 \le \varphi \le \pi + 2\alpha) \\ \pi & (\pi + 2\alpha \le \varphi \le 2\pi). \end{cases} \end{aligned}\right\} \tag{26}$$

The direction Θ of the velocity jumps by an amount π at the stagnation point where the velocity vanishes. The real part of (26) for known a_m, b_m and an angle of attack α gives the velocity $v(\varphi)$ at which this α occurs. On the other hand, if a function $v(\varphi)$ is prescribed with a corresponding α at which $v(\varphi)$ is to occur, then because of

$$P(\varphi) = \ln 2 \cos\left(\frac{\varphi}{2} - \alpha\right) - \ln v(\varphi) \tag{27}$$

the corresponding coefficients a_m, b_m can immediately be obtained by harmonic analysis. The derived conditions for a_0, b_0, a_1 b_1 are transferred using Equations (24) and (27) to the specified $v(\varphi)$. The quantity b_0 does not occur in $P(\varphi)$, and therefore (17) has nothing to do with the specification of $v(\varphi)$. It follows from Equations (22), (18), and (19) using the formulas for the Fourier coefficients

$$\int_0^{2\pi} P(\varphi)\, d\varphi = 0, \tag{28}$$

/36

$$\int_0^{2\pi} P(\varphi) \cos\varphi\, d\varphi = \pi, \tag{29}$$

$$\int_0^{2\pi} P(\varphi) \sin\varphi\, d\varphi = 0. \tag{30}$$

If a distribution $v(\varphi)$ has been found for an angle of attack α which satisfies (28) — (30), then the other a_m, b_m can be determined. These can be substituted in (16) and the mapping can be found by integration

$$z(\zeta) = \int \left(1 - \frac{1}{\zeta}\right) e^{\sum_{m=1}^{\infty} (a_m + ib_m)\zeta^{-m}} d\zeta \tag{31}$$

which then results in the entire flow in the z plane. The profile of this flow is the image of the unit circle. If $\zeta = e^{i\varphi}$ is introduced in Equation (31), then using (24), (25), and (27), after decomposing into a real and imaginary part according to (4), we have

$$x(\varphi) = \int -4 \sin\frac{\varphi}{2} \left|\cos\left(\frac{\varphi}{2} - \alpha\right)\right| \frac{1}{v(\varphi)} \cos\left(\frac{\varphi}{2} + Q(\varphi)\right) d\varphi, \tag{32}$$

$$y(\varphi) = \int -4 \sin \frac{\varphi}{2} \cos\left(\frac{\varphi}{2} - \alpha\right) \frac{1}{r(\varphi)} \sin\left(\frac{\varphi}{2} + Q(\varphi)\right) d\varphi . \tag{33}$$

This means that from the prescribed distribution $r(\varphi)$, it is only necessary to calculate the function $Q(\varphi)$ and in this way the corresponding profile is obtained with (32) and (33) in a parameter representation. $Q(\varphi)$ is the conjugate harmonic function of $P(\varphi)$, defined by the integral [4]

$$Q(\varphi) = \frac{1}{2\pi} \int_0^{2\pi} P(\sigma) \operatorname{ctg} \frac{\sigma - \varphi}{2} d\sigma \tag{34}$$

The lift of the profile is given as follows as a function of the circulation Γ according to (3) and because of the Kutta-Joukowski law (ϱ = density of the flow medium)

$$A = \varrho V \Gamma = \varrho \cdot 4\pi \sin \alpha, \tag{35}$$

and the lift coefficient is

$$c_a = \frac{A}{\frac{\varrho}{2} V^2 l} = 8\pi \sin \alpha \cdot \frac{1}{l}, \tag{36}$$

if l is the length of the profile. For the flat plate, we have

$$c_a = 2\pi \sin \alpha, \tag{37}$$

and it must be contained in the formulas for

$$l = 4 \tag{38}$$

For profiles with non-zero thickness, c_a is somewhat greater than (37) [5]. This leads to somewhat smaller l values than in (38), and we have

$$\frac{l}{4} \approx 1. \tag{39}$$

For $\alpha = 0$, c_a vanishes and the profile as a zero left direction parallel to the x axis.

The moment of the aerodynamic forces with respect to the origin according to H. Glauert [6] measured positive in the mathematically negative direction, is given by

$$M = \frac{1}{2} \varrho R_e \left\{ \oint \left(\frac{dF}{dz} \right)^2 z \, dz \right\}, \tag{40}$$

where the integration path must surround the profile in the mathematically positive direction. For $\alpha = 0$, that is for zero lift, we find the zero moment if we substitute our trial solution /37

$$M_0 = \frac{1}{2} \varrho 4\pi b_2, \tag{41}$$

the coefficient is

$$c_{m0} = \frac{M_0}{\frac{1}{2} \varrho V^2 l^2} = \frac{4\pi b_2}{l^2}, \tag{42}$$

where b_2 is the coefficient of the Fourier series $P(\varphi)$

$$b_2 = \frac{1}{\pi} \int_0^{2\pi} P(\varphi) \sin 2\varphi \, d\varphi \tag{43}$$

If we carry out the transition from $P(\varphi)$ to $Q(\eta)$ using (34) without the a_m, b_m, then b_2 must be especially calculated for the moment.

Our trial solution is equivalent to the trial solution having the form (6) and makes it possible to calculate a profile including lift and moment corresponding to any velocity profile $v(\varphi)$. A closed profile will be obtained with certainty, if (29) and (30) are satisfied. Equations (22) or (28) guarantee that $v(\varphi)$ belongs to the incident velocity V = 1, which can always be obtained by multiplying $v(\varphi)$ with a constant factor. This does not influence (29) and (30).

3. The Introduction of the Velocity Distribution

The formulas given above have solved the problem of calculating the profile from a velocity distribution. It is possible to prescribe an α or a c_a, because of (36), for which an arbitrarily selected velocity distribution $v(q)$ is to occur, and from this the profile can be calculated using (28) to (30), a test can be made whether a closed profile is produced and whether $v(q)$ corresponds to the incident velocity $V = 1$. However, this does not guarantee that the selected quantities will lead to a physically reasonable profile. This can only be tested using the numerical results.

We will now introduce $v(q)$ in a suitable form using suitable parameters. This form will describe general profile design problems in a simple way. The conditions (28) to (30) are satisfied using the parameters without any testing. The most important possibility of unreasonable profiles is excluded to begin with.

We already mentioned that, in the practical numerical evaluation of the formulas, we depend on the convergence of the series contained in (14). This is obtained by a corresponding selection of the function $v(q)$. We require that it makes $P(q)$ a piecewise analytical function according to (27), which at the most contains singularities which are inflection points, that is, which have a finite jumps in the first derivative. In this case, the a_m, b_m have the order $1/m^2$ [7], which can be numerically handled and which, at the same time, guarantees sufficiently smooth profiles.

This assumption is a very general one. The only important restriction is the continuity of $v(q)$ at the trailing edge $q = 0$. This continuity can no longer be avoided, as was possible in the

vortex distribution theory and in a certain sense also in the preceding paper [1]. The singularity produced by a discontinuity are in $P(\varphi)$ would now be too strong. In addition, our assumption according to (27) requires that at $\varphi = \pi + 2\alpha$, $v(\varphi)$ vanishes; this is the front stagnation point. Otherwise, $v(\varphi)$ cannot vanish anywhere, in particular at the trailing edge $\varphi = 0$. We therefore obtain the mentioned trailing edge angle $\delta = 0$.

It is possible to define unreasonable profiles within the framework of this restriction. For example, they can even cross over. We do not exclude them by any general formula condition. They are easily avoided in practice (see Section 5d).

We would like to take advantage of our formulas when the velocity distribution is finally introduced. Up to the present, they have been derived in such a way that a fixed angle of attack α is selected and a distribution $v(\varphi)$ which satisfies (28) to (30) is also selected. Then, using Equations (32) and (33), a profile is calculated whose velocity distribution $v(\varphi, \alpha)$ because of (26) agrees with the prescribed $v(\varphi)$ at the selected angle of attack α. However, there is a more general problem in practical aerodynamics. It is often not terribly important to be able to pre- /38
scribe $v(\varphi)$ for a fixed α or c_a over the entire profile. Usually it is desired to have entire angle of attack regions with favorable properties.

The most important related problem occurs in the calculation of so-called laminar profiles. In these calculations, one prescribes a non-decreasing velocity over an entire c_a range between two values $c_{a0} < c_{a1}$ along the upper side and the bottom side on the front stagnation point up to a certain point. Otherwise, the laminar boundary layer becomes unstable. In the ideal case, the velocity becomes constant over the corresponding part of the

top side c_{a1} and constant over the corresponding part of the bottom side c_{a0}.* This means that, according to the previous interpretation of our formulas, it is necessary to prescribe $v(\varphi)$ at an angle of attack α_1 which corresponds to a c_{a1}. Along the top side, a constant $v(\varphi)$ must be assumed over a short interval. Over the bottom side, we must have a variable $v(\varphi)$, out of which only the velocity change due to the angle of attack change up to c_{a0} brings about an interval with constant velocity.

The simultaneous observance of a second c_a or α is very simple here, even though it was difficult earlier. According to (15), the a_m, b_m determine the mapping $z(\zeta)$, that is the shape of the profile. If we assume a fixed profile, that is a_m, b_m and only change the angle of attack of the initial flow in the ζ plane in (3) and (2), then this does not change the mapping $z(\zeta)$. Because of (12) and (14), only the velocity in the z plane changes, therefore, also at the profile. This change can be most easily seen using (27). Because of (24) and for fixed a_m, b_m, $P(\varphi)$ is not allowed to change. That means that, for two different angles of attack α_1 and α,

$$-\ln v(\varphi,\alpha_1)+\ln 2\cos\left(\frac{\varphi}{2}-\alpha_1\right)=-\ln v(\varphi,\alpha)+\ln 2\cos\left(\frac{\varphi}{2}-\alpha\right). \qquad (44)$$

This means that, for a profile defined by $v(\varphi,\alpha)$ and α, it is easy to compute $v(\varphi,\alpha_1)$ for any φ without knowing the profile. Conversely, for any φ range, one can directly select $v(\varphi,\alpha_1)$ and from this calculate from (44) how $v(\varphi,\alpha)$ must be specified so that for the angle of attack α_1, one obtains the desired velocity

*See Figures 4 and 7, but also I. H. Abbott, A. E. v. Doenhoff, L. S. Stivers, Summary of Airfoil Data. NASA Report 824, Washington, 1945.

$v(\varphi, \alpha_1)$ there. If (44) is substituted in (27), we obtain the old equation, but it contains α_1 instead of α.

In general, just as in the preceding paper, $\alpha = \alpha^*(\varphi)$ can be specified as a (practically piecewise constant) function of φ and then form a distribution $v^*(\varphi)$ with it

$$P(\varphi) = \ln 2 \cos\left[\frac{\varphi}{2} - \alpha^*(\varphi)\right] - \ln v^*(\varphi) \tag{45}$$

Because of (24), certain a_m, b_m and a concrete profile are defined. As can easily be seen, it is calculated from (32) and (33) if we write $\alpha^*(\varphi)$ instead of α and $v^*(\varphi)$ instead of $v(\varphi)$, that is, without any formal change. The velocity distribution of the profile which is produced is as follows for a fixed α due to the relationship which follows from (27)

$$v(\varphi, \alpha) = 2\left|\cos\left(\frac{\varphi}{2} - \alpha\right)\right| e^{-P(\varphi)} \tag{46}$$

where (45)

$$v(\varphi, \alpha) = \left|\frac{\cos\left(\frac{\varphi}{2} - \alpha\right)}{\cos\left[\frac{\varphi}{2} - \alpha^*(\varphi)\right]}\right| v^*(\varphi). \tag{47}$$

This means that it agrees with the prescribed $v^*(\varphi)$ where the selected α agrees with the prescribed $\alpha^*(\varphi)$. We therefore obtain with $\alpha^*(\varphi)$ in certain φ regions, and therefore over certain profile parts the angle of attack α or lift coefficient c_a for which the prescribed $v^*(\varphi)$ occurs as a velocity.

The function $P(\varphi)$ according to (45) cannot have a jump according to our assumption. For example, if at a point φ_i there is a jump in the angle of attack $\alpha^*(\varphi)$ from α_i to $\alpha_i + 1$, then

because of

$$\lim_{\Delta\varphi\to 0}\left[-\ln v^*(\varphi+\Delta\varphi)\right]+\ln 2\left|\cos\left(\frac{\varphi}{2}-\alpha_{i+1}\right)\right|=\lim_{\Delta\varphi\to 0}\left[-\ln v^*(\varphi-\Delta\varphi)\right]+\ln 2\left|\cos\left(\frac{\varphi}{2}-\alpha_i\right)\right| \tag{48}$$

or

/39

$$\lim_{\Delta\varphi\to 0}\frac{v^*(\varphi+\Delta\varphi)}{v^*(\varphi-\Delta\varphi)}=\frac{\left|\cos\left(\frac{\varphi}{2}-\alpha_{i+1}\right)\right|}{\left|\cos\left(\frac{\varphi}{2}-\alpha_i\right)\right|} \tag{49}$$

$v^*(\varphi)$ must also have a jump. Equation (49) also assures the continuity of $v(\varphi,\alpha)$ for every α according to (47).

In this way, the mentioned problem of laminar profiles can be directly solved, by selecting $\alpha^*(\varphi)=\alpha_1$ along the corresponding part of the top side; we select $\alpha^*(\varphi)=\alpha_0$ in the appropriate bottom side interval and we also prescribe constant $v^*(\varphi)$. In order to treat such problems and even more general ones, we will have a special trial solution for $\alpha^*(\varphi)$ and $v^*(\varphi)$. We will first do this formally and will satisfy all of the conditions derived up to the present. In Section 4 we will describe the numerical calculation procedure. In Section 5 we will show what the trial solution can do. It can do quite a lot, but in spite of this, it is a special trial solution and cannot easily be replaced by another one.

We will divide the interval (0, 2π) into six parts, and we have the following equations for the limits

$$\varphi_0=0<\varphi_1<\varphi_2<\varphi_3<\varphi_4<\varphi_5<\varphi_6=2\pi \tag{50}$$

In the individual intervals, we specify that

$$\alpha^*(\varphi)=\alpha_i=\text{const}\qquad(\varphi_{i-1}\leqq\varphi\leqq\varphi_i) \tag{51}$$

For this, we set $v^*(\varphi)$ in the form

$$v^*(\varphi) = v_i w_i^{K_i}(\varphi) \qquad (\varphi_{i-1} \leqq \varphi \leqq \varphi_i) \tag{52}$$

where the v_i and K_i are free parameters. We will assume constant $v^*(\varphi)$ in the four middle segments. Therefore, we can set

$$K_2 = K_3 = K_4 = K_5 = 0 \tag{53}$$

The two other segments represent the surroundings of the trailing edge. Here there is always a velocity drop for profiles having a usable thickness. And its shape can be varied by means of the functions $w_1(\varphi)$ and $w_6(\varphi)$.

In the selection of $w_1(\varphi)$ and $w_6(\varphi)$, we will consider the continuity conditions specified by $P(\varphi)$ within the definition intervals. In addition, these functions cannot vanish anywhere. This means that of the free variables in (52), we must only have the continuity of

$$P(\varphi) = \ln\left|\cos\left(\frac{\varphi}{2} - \alpha_i\right)\right| - \ln v_i - K_i \ln w_i(\varphi) + \ln \Sigma, \quad (\varphi_{i-1} \leqq \varphi \leqq \varphi_i), \quad (i = 1, 2, \ldots 6) \tag{54}$$

at the points φ_i and must satisfy the conditions (28) to (30). We assume the following for $w_1(\varphi)$ and $w_6(\varphi)$

$$w_1(\varphi_1) = w_6(\varphi_5) = 1 \tag{55}$$

Then the continuity of $P(\varphi)$ at the point $\varphi_0 = 0$, according to (54) or $\varphi_6 = 2\pi$, respectively, requires

$$\ln|\cos\alpha_1| - \ln v_1 - K_1 \ln w_1(0) = \ln|\cos\alpha_6| - \ln v_6 - K_6 \ln w_6(2\pi), \tag{56}$$

and at the other points,

$$\ln\left|\cos\left(\frac{\varphi_i}{2} - \alpha_i\right)\right| - \ln v_i = \ln\left|\cos\left(\frac{\varphi_i}{2} - \alpha_{i+1}\right)\right| - \ln v_{i+1} \qquad (i = 1, 2, \ldots 5). \tag{57}$$

We will also cover the wing nose $\varphi \approx \pi$ with this piecewise constant $v^*(\varphi)$. In this region, $P(\varphi)$ can become infinite, if we have

$$\varphi = \pi + 2\alpha_i \tag{58}$$

in any interval. This must be avoided because of the assumptions made in this section for $P(\varphi)$. Therefore, it is appropriate to divide up our φ intervals in such a way that three of them are on the top side and three of them are on the bottom side of the profile. Because of (8), we then have $\varphi_3 \approx \pi$. In order that (58) does not occur in (54), we specify that

$$\alpha_3 > \alpha_4 \tag{59}$$

and

$$\pi + 2\alpha_4 < \varphi_3 < \pi + 2\alpha_3. \tag{60}$$

Together with Equations (56) and (57), we now have six equations for the six v_i. If, in Equations (50) and (51), we fix all φ_i and α_i, then in $P(\varphi)$, only the K_1 and K_6 are free to satisfy (28) to (30), which is not sufficient. This means that one of the quantities φ_i, α_i must be held free. φ_3 is best suited for this. By selecting $v^*(\varphi)$ and $\alpha^*(\varphi)$ and because of (47), for each α an entire distribution $v(\varphi, \alpha)$ and therefore a lift is specified. Because of (35), this must coincide with the one specified by α, which is guaranteed by (28) to (30). For closed profiles, (35) is valid. Therefore, we can satisfy (28) to (30) if the additional free variable has a large influence on the lift. This is especially true for φ_3, then according to Equation (57), v_3/v_4 and therefore the velocity ratio between the top side and the lower side is very sensitive to it. (Within the framework of (60), all positive values of v_3/v_4 can be

/40

achieved with φ_3.) All other φ_i and α_i would not be as well suited, and in addition, they are required later on for introducing design characteristics. Therefore, we will hold φ_3 free.

Accordingly, we now substitute (54) in (29) and (30). These integrals can be integrated in closed form, except for the parts

$$-\int_{\varphi_{i-1}}^{\varphi_i} \cos\varphi \ln w_i(\varphi)\, d\varphi = W_{ci}, \tag{61}$$

$$-\int_{\varphi_{i-1}}^{\varphi_i} \sin\varphi \ln w_i(\varphi)\, d\varphi = W_{si}, \tag{62}$$

about which we can say nothing without the $w_i(\varphi)$. We have

$$\int \cos\varphi \ln\left|\cos\left(\frac{\varphi}{2}-\alpha_i\right)\right| d\varphi = (\sin\varphi + \sin 2\alpha_i)\ln\left|\cos\left(\frac{\varphi}{2}-\alpha_i\right)\right| + \frac{1}{2}(\varphi\cos 2\alpha_i - \sin\varphi) + \text{Const.} \tag{63}$$

and

$$\int \sin\varphi \ln\left|\cos\left(\frac{\varphi}{2}-\alpha_i\right)\right| d\varphi = -(\cos\varphi + \cos 2\alpha_i)\ln\left|\cos\left(\frac{\varphi}{2}-\alpha_i\right)\right| + \frac{1}{2}(\varphi\sin 2\alpha_i + \cos\varphi) + \text{Const.} \tag{64}$$

Therefore, we have in (29),

$$\int_0^{2\pi} \cos\varphi\, P(\varphi)\, d\varphi = K_1 W_{c1} + K_6 W_{c6} + \sum_{i=1}^{6}\left\{\sin 2\alpha_i \ln\left|\frac{\cos\left(\frac{\varphi_i}{2}-\alpha_i\right)}{\cos\left(\frac{\varphi_{i-1}}{2}-\alpha_i\right)}\right| + \frac{1}{2}(\varphi_i-\varphi_{i-1})\cos 2\alpha_i \right.$$
$$\left. + \frac{1}{2}(\sin\varphi_i - \sin\varphi_{i-1}) + \sin\varphi_i\left[\ln\left|\cos\left(\frac{\varphi_i}{2}-\alpha_i\right)\right| - \ln v_i\right] - \sin\varphi_{i-1}\left[\ln\left|\cos\left(\frac{\varphi_{i-1}}{2}-\alpha_i\right)\right| - \ln v_i\right]\right\}. \tag{65}$$

The next to the last term with i and the last term with i + 1 cancel in the summation because of (57). Only the last term with i = 1 remains of these two terms, as well as the next to the last one with i = 6, which vanishes because of the sin factors. The members of the third term also vanish after summation, so that

$$\int_0^{2\pi} P(\varphi)\cos\varphi\, d\varphi = K_1 W_{c1} + K_6 W_{c6} + \sum_{i=1}^{6}\left\{\sin 2\alpha_i \ln\left|\frac{\cos\left(\frac{\varphi_i}{2}-\alpha_i\right)}{\cos\left(\frac{\varphi_{i-1}}{2}-\alpha_i\right)}\right| + \frac{1}{2}(\varphi_i-\varphi_{i-1})\cos 2\alpha_i\right\} \tag{66}$$

We will introduce the abbreviation J_c for the sum, and for the logarithms

$$\ln\left|\cos\left(\frac{\varphi_i}{2}-\alpha_j\right)\right| = \ln(i,j). \tag{67}$$

If we collect terms containing φ_i, we find the following quantity required in (29)

$$J_c-\pi=\sum_{i=0}^{6}\left\{\sin 2\alpha_i \ln(i,i)-\sin 2\alpha_{i+1}\ln(i,i+1)+\frac{1}{2}\varphi_i(\cos 2\alpha_i-\cos 2\alpha_{i+1})\right\}, \tag{68}$$

and formally we must set

$$\alpha_0=\alpha_7=0 \tag{69}$$

which have not yet been defined. In a similar way, we use (64) /41 to find the integral required for (30)

$$\int_0^{2\pi}\sin\varphi\,P(\varphi)\,d\varphi = K_1W_{s1}+K_6W_{s6}+\sum_{i=1}^{6}\left\{-\cos 2\alpha_i\ln\left|\frac{\cos\left(\frac{\varphi_i}{2}-\alpha_i\right)}{\cos\left(\frac{\varphi_{i-1}}{2}-\alpha_i\right)}\right|+\frac{1}{2}(\varphi_i-\varphi_{i-1})\sin 2\alpha_i\right.$$
$$\left.+\frac{1}{2}(\cos\varphi_i-\cos\varphi_{i-1})-\cos\varphi_i\left[\ln\left|\cos\left(\frac{\varphi_i}{2}-\alpha_i\right)\right|-\ln r_i\right]+\cos\varphi_{i-1}\left[\ln\left|\cos\frac{\varphi_{i-1}}{2}-\alpha_i\right|-\ln r_i\right]\right\}. \tag{70}$$

Here again we have the same simplifications as above, but now the last term with i = 1 as well as the next to the last one with i = 6 do not vanish. If we call J_s the sum of (70) and introduce the abbreviation (67), then we have

$$J_s=\sum_{i=1}^{6}\left\{-\cos 2\alpha_i[\ln(i,i)-\ln(i-1,i)]+\frac{1}{2}(\varphi_i-\varphi_{i-1})\sin 2\alpha_i\right\} \tag{71}$$
$$+\ln(0,1)-\ln v_1-\ln(6,6)+\ln r_6.$$

From this, we eliminate v_1 and v_6 by continuous application of (57), which results in

$$J_s=\sum_{i=1}^{6}\left\{-(1+\cos 2\alpha_i)[\ln(i,i)-\ln(i-1,i)]+\frac{1}{2}(\varphi_i-\varphi_{i-1})\sin 2\alpha_i\right\} \tag{72}$$

The conversion analogous to (68) gives

$$J_s = \sum_{i=0}^{6} \left\{ -(1+\cos 2\alpha_i)\ln(i,i) + (1+\cos 2\alpha_{i+1})\ln(i,i+1) + \frac{1}{2}\varphi_i(\sin 2\alpha_i - \sin 2\alpha_{i+1}) \right\}, \quad (73)$$

which again is correct considering (69). This means that we have the following closure equations (29) and (30)

$$K_1 W_{c1} + K_6 W_{c6} + J_c - \pi = 0, \quad (74)$$

$$K_1 W_{s1} + K_6 W_{s6} + J_s = 0. \quad (75)$$

From (56) we also eliminate v_1 and v_6 by continuous application of (57). If we consider (69) and introduce

$$J_t = \sum_{i=0}^{6} \{-\ln(i,i) + \ln(i,i+1)\} \quad (76)$$

we find

$$-K_1 \ln w_1(0) + K_6 \ln w_6(2\pi) + J_t = 0. \quad (77)$$

Equations (74), (75), and (77) contain the only unknowns K_1, K_6, and φ_3. They can be determined from these equations. First, we eliminate K_1 and K_6 and find

$$(J_c - \pi) D_1 - J_s D_2 + J_t D_3 = 0 \quad (78)$$

where

$$D_1 = W_{s1} \ln w_6(2\pi) + W_{s6} \ln w_1(0), \quad (79)$$

$$D_2 = W_{c1} \ln w_6(2\pi) + W_{c6} \ln w_1(0), \quad (80)$$

$$D_3 = W_{c1} W_{s6} - W_{c6} W_{s1}. \quad (81)$$

Equation (78) is a transcendental equation for φ_3 of the type

$$a + b \log \left|\cos\left(\frac{\varphi_3}{2} - \alpha_3\right)\right| + c \log \left|\cos\left(\frac{\varphi_3}{2} - \alpha_4\right)\right| + d \cdot \varphi_3 = 0, \tag{82}$$

and the constants a, b, c, d can be calculated from Equations (68), (73), (76), and (79) to (81). We will do this in the following section in detail. From (82), φ_3 is determined using well-known methods. This means that the J_c, J_s, and J_t can be determined according to (68), (73), and (76), from which it follows that

$$K_1 = \frac{1}{D_1}(-\ln w_6(2\pi)\, J_s + W_{s6} J_t), \tag{83}$$

$$K_6 = \frac{1}{D_1}(-\ln w_1(0)\, J_s - W_{s1} J_t) \tag{84}$$

In order to determine the v_i, in addition to the five equations (57), we need another equation. It follows from Equation (28), which has not yet been used /42

$$\int_0^{2\pi} P(\varphi)\, d\varphi = \sum_{i=1}^{6} \left\{ \int_{\varphi_{i-1}}^{\varphi_i} \left[\ln \left|\cos\left(\frac{\varphi}{2} - \alpha_i\right)\right| - \ln \frac{r_i}{r_1} - K_i \ln w_i(\varphi) \right] d\varphi \right\} + 2\pi (\ln 2 - \ln v_1) = 0. \tag{85}$$

Here the velocity ratios can be found from (57), φ_3 and the K_i are already known. This means that a v_1 value is defined from which the other v_i values can be calculated using (57).

Our trial solution now consists of any selection of the $w_i(\varphi), \alpha_i$ and φ_i and φ_3 a permissible function $P(\varphi)$. This means that a profile is defined with (32) and (33). We will also give the numerical calculation for finding the profile. In Section 5 we will show what the trial solution does for practical problems.

4. The Practical Numerical Calculation

The practical calcululation of our method essentially consists of three different parts. First, the function $P(\varphi)$ must be calculated using (54) with all the constants. Ther $Q(\varphi)$ is found from (34), and then the integrations (32) and (33) are carried out.

We will divide the interval (0, 2π) into 2N parts and will consider the points

$$\varphi = \tau_\nu = \nu \frac{\pi}{N} \qquad (\nu = 0, 1, 2, \ldots, 2N-1). \tag{86}$$

The even number N cannot be too small, if we are too have a good accuracy for the method. Therefore, it is not a restriction if we select the positions φ_i (except for φ_3) of (50) at certain points τ_ν. In addition to the φ_i, we will assume that the α_i of (51) and the $w_i(\varphi)$ of (52) are given.

During our calculation we require the following functions at the points τ_ν, which will be mentioned now:

a) $\log\left|\cos\left(\frac{\tau_\nu}{2}-\alpha_i\right)\right|$ but only between φ_{i-1} and φ_i in order to form $P(\varphi)$,

b) $\cos\left(\frac{\tau_\nu}{2}-\alpha_i\right)$ for all α_i and all τ_ν for Equations (32), (33), and (47),

c) $\sin\frac{\tau_\nu}{2}$ for (32) and (33),

d) $\log w_i(\varphi)$ for $P(\varphi)$ and the integrals (61) and (62).

The base ten logarithms are sufficient. Only occasionally do we have to transfer to natural logarithms by multiplying ln 10. The point φ_3 is not yet known. Therefore, the regions containing α_3 and α_4 are first limited by an adjacent value τ_r, which can be specified according to (60). At the other integral limits, we find the logarithms required for the ln (i, j) according to (67), which according to (67) are called

$$\log \cos\left(\frac{\varphi_i}{2} - \alpha_j\right) = \log (i, j) \tag{87}$$

The integrals W_{si} and W_{ci} according to (6 nd (62) can be evaluated in closed form, depending on the sele n of the functions $w_i(\varphi)$, or the interpolation methods can be used to determine it from the values

$$\cos\tau_r \log w_i(\tau_r), \quad \sin\tau_r \log w_i(\tau_r)$$

[8]. The values $\cos\tau_r$ and $\sin\tau_r$ are contained in the values of $\sin\tau_r/2$. In the result, we must consider the factor -ln 10.

Using the W_{si}, W_{ci} and the other quantities in Equations (79) to (81), except for the factor ln 10, we form the D_i for that location. The transcendental equation (82) is best established in the following sequence. First the quantities of the equation

$$J_c - \pi = a_c + b_c \log (3, 3) + c_c \log (3, 4) + d_c \varphi_3 \tag{88}$$

is calculated where a_c is the sum (68) without the term with i = 3, b_c, c_c, and d_c are the contributions of the term i = 3. In a similar way, according to (73), the quantites a_s, b_s, c_s, and d_s are calculated for J_s. The a_t, b_t, and c_t are calculated according to (76). d_t vanishes. All these variables can easily

be calculated using the already available log (i, j) and the few /43 values sin 2 α_i, cos 2 α_i, and φ_i (in arc units). With them, the quantities a, b, c, d required in (82) are found as follows

$$a = D_1 a_c - D_2 a_s + D_3 a_t \tag{89}$$

and similarly, the b, c, d.

The transcendental equation (82) for φ_3 is best solved using the Regula falsi Equation (60) gives an indication of the initial approximation for φ_3. There is a small amount of effort associated with this.

The solution of (82) automatically also results in the log (3, 3), log (3, 4) and φ_3 and correspondingly according to Equation (88), one calculates the $J_c - \pi$, J_s and J_t and then the K_1 and K_6 using (83) and (84). As a check, the numbers obtained are substituted in Equation (74).

By solving the system of equations (74), (75), (77), the following values are easily found

$$P_\nu = \bar{P}(\tau_\nu) = \log\left|\cos\left(\frac{\tau_\nu}{2} - \alpha_i\right)\right| - \log\frac{v_i}{v_1} - K_i \log w_i(\tau_\nu), \tag{90}$$

and the most important numbers for this are already available. In particular, because of (57), it is possible to calculate the

$$\log\frac{v_{i+1}}{v_i} = \log(i, i+1) - \log(i, i) \tag{91}$$

from the log (i, j). The relationship between the numbers from (90) and $P(\varphi)$ is as follows

$$P_\nu = P(\tau_\nu) = \ln 10\,(P(\tau_\nu) + \log 2 - \log v_1). \tag{92}$$

It does not have to be calculated explicitly, because in the transfer from (34) to $Q(q)$, an additional constant does not play any role. The multiplication constant will be taken along in the calculation of $Q(q)$ in (34).

Equation (34) is evaluated in the well-known manner [4], by interpolating the $P(\tau_\nu)$ using a trigonometric polynomial having 2 N coefficients. We then transfer to the conjugate form according to (24) and (25). Then $Q(q)$ is again summed at the points $q = \tau_\nu$. This process can be represented in the following simple form

$$\tau_\nu \cdots Q(\tau_\nu) = \frac{1}{N} \sum_{\mu=1}^{N-1} (P_{\nu+\mu} - P_{\nu-\mu}) \operatorname{ctg} \frac{\mu\pi}{2N} \qquad (\mu \text{ odd}) \tag{93}$$

In Equations (32) and (33), $Q(q)$ is required in degrees, because special tables are available for it.* In addition, at the position P_ν we require the P_ν of (90). Therefore, we have

$$Q_\nu = \sum_{\mu=1}^{N} (\bar{P}_{\nu+\mu} - \bar{P}_{\nu-\mu}) k_\mu, \qquad (\bar{P}_{\nu+2N} = \bar{P}_\nu) \tag{94}$$

and the factors

$$k_\mu = \begin{cases} \dfrac{180^\circ \ln 10}{\pi N} \operatorname{ctg} \dfrac{\mu\pi}{2N}, & (\mu \quad \text{odd}) \\ 0 & (\mu \quad \text{even}) \end{cases} \tag{95}$$

can be calculated for a selected N. Table 1 shows the values for N = 24 and N = 30.

---

*The best tables are these of A. Danjon, Tables of Trigonometric Functions, Natural Values to Six Decimals in Units of One Hundredths, Paris, 1948.

TABLE 1*

THE k_μ FOR N = 24 AND N = 30

$N = 24$		$N = 30$	
μ	k_μ [ ]	μ	k_μ [ ]
1	83,86828	1	83,91147
3	27,63537	3	27,76544
5	16,19369	5	16,41212
7	11,14685	7	11,45617
9	8,22687	9	8,63080
11	6,26814	11	6,77173
13	4,82075	13	5,43060
15	3,67299	15	4,39761
17	2,71083	17	3,56112
19	1,86598	19	2,85585
21	1,09312	21	2,24069
23	0,36029	23	1,68809
		25	1,17834
		27	0,69651
		29	0,23047

* Translator's Note: Commas in numbers indicate decimals.

The calculation of the Q_ν according to (94) is the main effort in the method. The number N cannot be selected too small, so that sufficient number of points are calculated over the profile. If we assume N = 24, which is a minimum requirement, then (94) requires 48 product sums, each having 12 sums and 12 products. If possible, large computers can be used here. The IBM punched card method has proven itself well.*

As a test on Q_ν, we can use the reversal of (94)

$$\sum_{\mu=1}^{N}(Q_{\nu+\mu}-Q_{\nu-\mu})\,k_\mu=-\left(\frac{180^\circ\ln 10}{\pi}\right)^2\left(\bar{P}_\nu-\frac{1}{N}\sum_{\sigma=0}^{N-1}\bar{P}_{\nu+2\sigma}\right). \qquad (96)$$

The last sum is the same for all odd and even ν, then the $\bar{P}_\nu$ are /44 periodic with the period 2 N.

*This work was done in collaboration with the Directorate of the Allianz-Lebensversicherungs A. G. at their Holerith Division, using an electronic computer-punch IBM 604. I'm thankful to the association and especially Dr. Kanngiesser, who provided the circuit.

Garrick [4] discussed the accuracy of (94). The accuracy is poor if the Fourier series of $P(\gamma)$ does not converge or only converges poorly. Lighthill [2] goes directly from the function $\ln c(\varphi)$, which has a singularity at the stagnation point, to the conjugate harmonic function, which is only possible in special cases, using the improper integral (34) and various specially tabulated integral functions. Our modified method makes it possible to satisfy the previous continuity requirements and therefore to apply (94) with sufficient accuracy.

Only the function $s^*(\varphi)$ according to (52) remains to be determined for the integrands of (32) and (33). We will write them in the form

$$s^*(\gamma) = c_1 \frac{c_i}{c_1} w_i^{K_i}. \tag{97}$$

The velocity ratios must be expressed in terms of the known log (i, j) because of (91). The $w_i^{K_i}$ can be calculated logarithmically from the already available functions log w_i. The quantity v_1 only enters (32) and (33) in a multiplication, and therefor, controls the scale of the z plane. The scale is only important because of the quantity $l/4$, of (36), which does not have to be too accurate. We will evaluate (85) approximately. Because of (92), we can also use the $\bar{P}_\nu$ instead of the P_ν. Then instead of (85), we obtain

$$\log c_1 = \log 2 + \frac{1}{2N} \sum_{\nu=1}^{2N} \bar{P}_\nu, \tag{98}$$

if we evaluate the integral using the simple rectangle formula. This is equivalent to the interpolation integration of arbitrary order, because when a periodic function is integrated over its period, the differences of higher order do not have any influence.*

*See also later on in the integration of (32) and (33).

We should like to note that (97) and (98) can be calculated before the transition from (94) is made to the Q_r. This means that, if the distributions $r(\varphi, x)$ which are the consequence of the selected trial variables are not clear, it is possible to calculate them from (97) and (47) before most of the numerical work is done. If they have any disadvantages (see also Section 5), then if necessary, the calculation can be started again with new input variables. If not all of the quantities are changed, it is possible to make use of some of the preceding calculations. For example, if we only change the $w_i(\varphi)$, then the a_c, b_c, c_c, d_c of (88) and the analog quantities J_s and J_t remain the same. On the other hand, if the $w_i(\varphi)$ are held fixed, then the D_i of (79) to (81) remain the same.

By means of (97) and (98), we can completely calculate the integrands of (32) and (33) point by point. We will not carry out this calculation, but will consider some practical problems instead.

First of all, in (32) and (33), we will omit the factor 4. Therefore, the profile has a length

$$l_1 = \frac{l}{4}, \tag{99}$$

from which we obtain the following from (36)

$$c_a = \frac{1}{l_1} \cdot 2\pi \sin\alpha \tag{100}$$

The profile obtained in this way has zero lift for $\alpha = 0$, /45 as we established earlier. Profiles with a large curvature, which are calculated for positive α or c_a, therefore have a front side which is greatly curved towards the bottom. This

can be avoided during the integration already, by reducing the inclination angle in (32) and (33) everywhere by the angle β. It can be determined from the calculated inclindation angles approximately how large β must be so that the nose and the trailing edge have the same height. The profile will then have zero lift at the new position for an angle of attack $\alpha = -\beta$.

Accordingly, instead of (32) and (33), for the integration at the points τ_ν, we will use the quantities

$$\dot{x}_\nu = \dot{x}(\tau_\nu) = -\sin\frac{\tau_\nu}{2}\left|\cos\left(\frac{\tau_\nu}{2} - \alpha_i\right)\right| \frac{1}{v^2(\tau)}\cos\left(\frac{\tau_\nu}{2} + Q_\nu - \beta\right), \tag{101}$$

$$\dot{y}_\nu = \dot{y}(\tau_\nu) = -\sin\frac{\tau_\nu}{2}\left|\cos\left(\frac{\tau_\nu}{2} - \alpha_i\right)\right| \frac{1}{v^2(\tau)}\sin\left(\frac{\tau_\nu}{2} + Q_\nu - \beta\right), \tag{102}$$

which we can easily calculate with results obtained up to the present.

The integration will also not yet be carried out, but first we will follow it through the calculation and will see which method of calculation will be the simplest in order to obtain the final result. We will form the first and second differences of (101) using the $\dot{x}_\nu$ according to Table 2, which are required for the integration by interpolation [8]. In order to obtain the second differences for $\nu = 0$, we extend the diagram backwards to $\nu = 2N-1$. If we set x(0) = 0, then we have

$$\left.\begin{aligned} x_1 = x(\tau_1) &\approx h\left[\frac{1}{2}(\dot{x}_0 + \dot{x}_1) - \frac{1}{24}(\Delta^2\dot{x}_0 + \Delta^2\dot{x}_1)\right], \\ x_2 = x(\tau_2) &\approx h\left[\frac{1}{2}(\dot{x}_1 + \dot{x}_2) - \frac{1}{24}(\Delta^2\dot{x}_1 + \Delta^2\dot{x}_2)\right] + x_1, \end{aligned}\right\} \tag{103}$$

and so on, where h is the difference of the argument

$$h = \frac{\pi}{N} \tag{104}$$

TABLE 2

DIFFERENCE DIAGRAM FOR THE INTEGRATION (103)

ν	$\dot{x}_\nu$	$\Delta\dot{x}_\nu$	$\Delta^2\dot{x}_\nu$
$2N-1$	$\dot{x}_{2N-1}$		$\Delta^2\dot{x}_{2N-1}$
0	$\dot{x}_0$	$\Delta\dot{x}_0$	$\Delta^2\dot{x}_0$
1	$\dot{x}_1$	$\Delta\dot{x}_1$	$\Delta^2\dot{x}_1$
2	$\dot{x}_2$	$\Delta\dot{x}_2$	$\Delta^2\dot{x}_2$
3	$\dot{x}_3$	$\Delta\dot{x}_3$	$\Delta^2\dot{x}_3$
4	$\dot{x}_4$	$\Delta\dot{x}_4$	$\Delta^2\dot{x}_4$
5	$\dot{x}_5$	$\Delta\dot{x}_5$	$\Delta^2\dot{x}_5$

This integration can easily be formulated in a continuous manner, and this is done by first doing the calculation with the functional values and later on using the second differences. The constant factors can then remain in the machine.

The function $x(q)$ which is produced must be periodic. If the profile is to close, we must have $x_0 = x_{2N}$. This will not be satisfied exactly, because approximate methods have been used for the integration and for calculating $Q(q)$. The difference which is produced

$$\varepsilon_x = x_{2N} - x_0 \tag{105}$$

is, on the one hand, a measure for the accuracy of the calculation, and a completely independent calculation check. If it is small enough, so that we are not made aware of a calculation error, then it can be compensated for in a simple way. The differences show clearly that the higher differences do not contribute anything to ε_x. Instead, we must have

$$S_x = \sum_{\nu=1}^{2N} \dot{x}_\nu = 0 \tag{106}$$

Therefore, we carry out the calculation as follows. First, using the variables in (101), we formulate S_x according to (106). The resulting error according to (103) is

$$\varepsilon_x = \frac{\pi}{N} S_x. \tag{107}$$

We use this error to judge the accuracy of the computation accuracy. Considering the boundary layer thickness at the trailing edge, we can certainly allow the following

$$\varepsilon_x \leqq 0.003\, l \tag{108}$$

that means, for a profile having a length of one meter, we can allow a horizontal displacement of 3 mm. If ε_x is small enough, then the $\dot{x}_\nu$ can be equalized by subtracting from all the $\dot{x}_\nu$ the quantity /46

$$\delta_x = \frac{S_x}{2N-1} \tag{109}$$

according to (101), except for the vanishing quantity $\dot{x}_0$. Then Equation (106) will certainly be satisfied and the function produced $x(\varphi)$ becomes periodic.

We will now form the first differences and calculate the x_ν according to (103), and we set $x_0 = 0$. Then, $x(\varphi)$ goes from zero to a minimum

$$x_{min} = -l_1 \tag{110}$$

and again back to zero. The quantity x_{min} is usually not assumed at the point x_ν in general. Therefore, $x(\varphi)$ is interpreted in the vicinity of the minimum by a parabola, and we take its minimum. Let x_κ be the smallest of the x_ν which are produced, then we have

$$-l_1 = x_N + \frac{(x_{N-1} - x_{N-3})^2}{8(2x_N - x_{N-1} - x_{N-3})}. \qquad (111)$$

Therefore, we can easily carry out the complete transformation

$$X_\nu = 100\left(\frac{x_\nu}{l_1} + 1\right) \qquad (112)$$

The function $x(\varphi)$ then goes from 100 to 0, as usual.

The corresponding function $Y(\varphi)$ is produced in a completely similar way. First we calculate S_y just like (106), and from this ε_y and δ_y. As far as ε_y is concerned, we must require a somewhat higher accuracy than for ε_x, which is usually required, say

$$\varepsilon_y \leq 0.002\, l. \qquad (113)$$

In the integration according to (103), instead of the quantity h, we will take the factor $100\frac{h}{l_1}$, so that the Y_ν immediately are located at the place corresponding to the X_ν.

According to (47), it is possible to completely calculate the distributions $v(\varphi, \alpha)$ and $v^2(\varphi, \alpha)$ for all α. The recalculation variables for the α_i used in $\alpha^*(\varphi)$ are already known. The zero moment according to (42) and (43) must be calculated. Instead of (43), we will use the approximation

$$b_2 = \frac{\ln 10}{N} \sum_{\nu=1}^{2N} \bar{P}_\nu \sin 2\tau_\nu, \qquad (114)$$

which corresponds to the accuracy of Equation (93).

The entire method therefore causes no difficulties in the numerical evaluation. A trained mathematician can carry out the calculation in about thirty hours without using a large computer, if he uses N = 24.

The selection of the quantity N depends on the required accuracy. However, it usually will not be selected larger than N = 30, because otherwise, the computation effort is too great. Instead, the accuracy of the result can be improved in another way. The greatest inaccuracy of our method is produced by the large bend in the function $P(\varphi)$ at the point $\varphi = \varphi_3$, which is not well interpolated by means of a trigonometric polynomial (see also Section 5, Figure 5). Since this interpolation is contained in (93), small fluctuations are produced in the Q_ν. They are completely smooth during the integration and no longer disturb the result. However, they primarily cause the errors ε_x and ε_y. If one wants to reduce them, then a closed part of $\bar{P}(\varphi)$ is split off before the transition to $Q(\varphi)$, which contains the large bend and for which (34) can be evaluated in close form. This can be done in the form

$$\bar{P}(\varphi) = k\left|\sin\left(\frac{\varphi - \varphi_3}{2}\right)\right| + \bar{P}^{(1)}(\varphi) \tag{115}$$

where

$$k = \frac{1}{2\ln 10}\left[\operatorname{tg}\left(\frac{\varphi_3}{2} - \alpha_3\right) - \operatorname{tg}\left(\frac{\varphi_3}{2} - \alpha_4\right)\right] \tag{116}$$

which leads to

$$Q(\varphi) = -\frac{2k}{\pi}\ln 10 \sin\left(\frac{\varphi - \varphi_3}{2}\right)\ln\left|\operatorname{tg}\left(\frac{\varphi - \varphi_3}{4}\right)\right| + Q^{(1)}(\varphi) \tag{117}$$

The function $\bar{P}^{(1)}(\varphi)$ has a continuous tangent at $\varphi = \varphi_3$ and $Q^{(1)}(\varphi)$ can be calculated from it using the derived formulas (94) and

/47

(95). This splitting off, in general, results in better improvement with less effort than an increase in N. Up to the present, it has not become necessary in any sample calculation.

Our trial solution therefore leads to our result with a reasonable amount of effort. We will also show what it can do for the profile calculation.

5. The Covered Profile Design Possibilities

Depending on how the quantities x_i, y_{ij} and $w_i(\varphi)$ of the preceding sections are selected, profiles with various characteristics are produced. In this section, we will give a qualitative description of the most important possibilities of profile design covered by our trial solution. In Section 6, we will give a numerical example.

The circle in the ζ plane has been divided into six parts by (50). Because of (8), which transform to normal coordinates X is

$$X \approx 50\,(1 + \cos\varphi) \tag{118}$$

we can vary the limits φ_i of (50) approximately over the limits $X_i = X(\varphi_i)$ of the corresponding regions of the profile. In our method, we have only specified φ_3. The point X_3 lies approximately at the profile nose $X_3 \approx 0$. This means that we have three regions each on the top side and the bottom side, and the boundaries can be arbitrarily selected.

Using (51), and because of (47), within the individual regions, we will select the angle of attack for which the $v^*(\varphi)$ of the trial solution (52) must appear as a velocity. Except for the first and the last region in (50), $v^*(\varphi) = v_i$ becomes constant

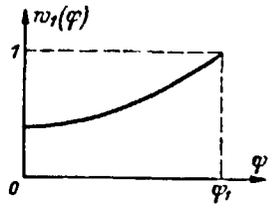

Figure 2. Approximate variation of a usable function $w_1(\varphi)$.

because of (53). In the two adjacent regions of the nose and the ones connected to it, we will therefore only select certain angles of attack α_i for which constant velocity is to be produced there. The quantity v_i for it will be determined by the method.

If we require only one such region with a constant velocity along the top side and the bottom side, then we select

$$\alpha_2 = \alpha_3, \qquad \alpha_4 = \alpha_5. \tag{119}$$

which, together with (57), results in

$$v_2 = v_3, \qquad v_4 = v_5 \tag{120}$$

The two regions then have the same velocity for the same angle of attack and, therefore, merge into one region. The points φ_2 and φ_3 therefore no longer have any influence and do no longer have to be fixed.

We will talk about the exact form of $w_1(\varphi)$. Since it must always produce a certain velocity drop at the trailing edge for normal thick profiles, we will first assume that $w_1(\varphi)$ has the form given in Figure 2, where, in addition to (55), we also have the favorable condition

$$\left(\frac{dw_1}{d\varphi}\right)_{\varphi=0} = 0 \tag{121}$$

so that no vertical tangent in v(X) occurs during the transition to X. In a similar way, we can introduce $w_0(\varphi)$.

We can almost always assume the following conditions for the angles of attack α_1 and α_6

$$\alpha_1 = \alpha_2, \quad \alpha_5 = \alpha_6 \tag{122}$$

which leads to the following according to (57)

$$v_1 = v_2, \quad v_5 = v_6 \tag{123}$$

By $w_1(\varphi)$ and $w_6(\varphi)$, we only will fix the form of the velocity decrease at the trailing edge at those angles of attack at which there is constant velocity in the preceding regions. The velocity drop then becomes proportional to the v_i according to (52), which must be considered in the selection of $w_i(\varphi)$.

We obtain symmetric profiles by means of a further specialization. For them, at $\alpha = 0$, the velocity on the top side and the bottom side is equal and, in addition, the mapping $z(\zeta)$ must be symmetric and we must have $X(\varphi) = X(-\varphi)$. This means that $v(\varphi, 0)$ and, according to (27), $P(\varphi)$ become even functions. In (24), all b_m vanish. In our trial solution, we have the following conditions because of the equations (50), (51), (52), (61), and (62) /48

$$\left.\begin{array}{lll} \alpha_1 = -\alpha_6, & \varphi_1 = 2\pi - \varphi_5, & w_1(\varphi) = w_6(2\pi - \varphi), \\ \alpha_2 = -\alpha_5, & \varphi_2 = 2\pi - \varphi_4, & W_{s1} = -W_{s6}, \\ \alpha_3 = -\alpha_4, & \varphi_3 = \pi, & W_{c1} = W_{c6}. \end{array}\right\} \tag{124}$$

We will now discuss some of the following possibilities of profile design.

a) Simple, symmetric laminar profiles

We will consider (124),

$$\alpha_1 = \alpha_2 = \alpha_3 > 0, \tag{125}$$

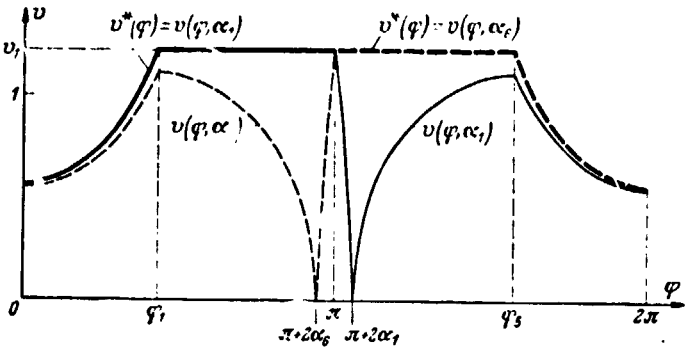

Figure 3. Functions $v^*(\varphi)$, $v(\varphi,\alpha_1)$ and $v(\varphi,\alpha_6)$ for a simple symmetric laminar profile (schematic).

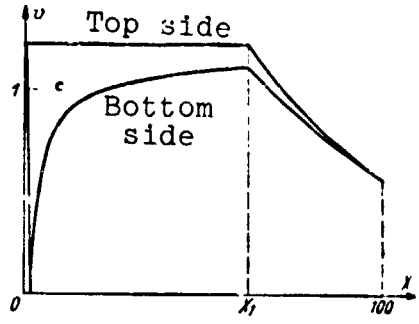

Figure 4. The function $v(X,\alpha_1)$ for a simple symmetrical laminar profile (schematic).

and will select a variable φ_1 which, according to (118) specifies the beginning X_1 of the velocity decrease, and we also select a $w_1(\varphi)$ approximately according to Figure 2 with (121). The calculation procedure of Section 4 for determining $P(\varphi)$ and $v^*(\varphi)$ then becomes automatic. Because of (57), we have

$$v_i = v_1 \tag{126}$$

for all i. The Equations (75) and (77) are satisfied by $\varphi_3 = \pi$ and $K_1 = K_6$. From (74), we obtain a K_1 and from (98), a v_1. According to (52), we find the distribution $v^*(\varphi)$ shown in Figure 3 (solid lines), which is symmetric with respect to $\varphi = \pi$ (47) and which results in the distributions $v(\varphi,\alpha_1)$ (solid lines) and $v(\varphi,\alpha_6)$ (dashed lines) also shown. If we make the transition to X, we find the variation $v(X,\alpha_1)$ shown in Figure 4, which corresponds exactly to the requirement for the known laminar profiles [9]. For the angle of attack α_1, the velocity at the top side is constant from the nose to X_1. For $\alpha_6 = -\alpha_1$, we have the same thing, but the lines for the top side and the bottom side are exchanged. For all angles of attack α between α_1 and $-\alpha_1$,

the velocity $u(X, y)$ (47) increases up to the point X_1 along the top side and the bottom side.

The final form of the velocity drop at the trailing edge ($X_1 < X < \infty$) depends on the selected function $u_1(\varphi)$ as well as the resulting quantity K_1, which appears as an exponent. From the standpoint of boundary layer theory, the form given by $u_1(\varphi)$ cannot be modified too much. Therefore, we are interested in having $K_1 \approx 1$. This can be done by selecting $u_1(\varphi)$ large enough according to the required velocity drop with $K_1 = 1$, which is easily done after a few examples are calculated. If a K_1 is produces which deforms the $u_1(\varphi)$ too much, then this will be noted already in the first calculation, the solution of Equation (82), which comes well before the main calculation effort. It is then easy to start again using a change $u_1(\varphi)$.

The symmetric profiles which can be calculated using the selection (125) approximately correspond to those of the NACA Report 824.* In this case, we can only change the shape of the velocity drop by means of $u_1(\varphi)$. In addition, the constant velocity at $x = x_1$ extends up to the nose $\varphi = \pi$, which could not be done completely for the NACA profiles. It may seem that this difference is inconsequential. However, if we go over to the function $P(\varphi)$ according to (27), then the influence becomes much greater because the immediate vicinity of the nose already fills /49 a considerable φ range. According to (54), because we use the function $P(\varphi)$ in our method, there is a bend (Figure 5) in the form of a tip at $\varphi = \pi$, because of the fact that the velocity $u(\varphi, x_1)$ was constant up to that point. This is because the

*See Footnote on p. 15.

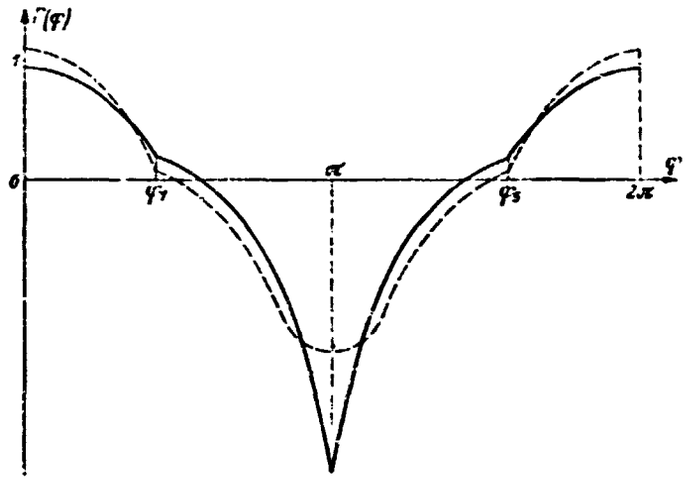

Figure 5. The improvement of the function $P(\varphi)$ for the present method (solid lines) compared with earlier methods (dashed lines).

argument of $\cos\left(\frac{\varphi}{2}-\varphi_1\right)$ comes close to $\pi/2$. This tip then makes a substantial contribution to the integral K_i. It disappears when $P(\varphi-\varphi_1)$ decreases towards the nose (dashed curve in Figure 5). In this case, all of the K and therefore the velocity decrease at the trailing edge must be greater in order for (74) to be satisfied. This means that a pressure increase along the back side can be saved by carefully shaping the nose.

The tip of $P(\varphi)$ in our numerical calculations is not exactly computed by the interpolation, but we will use more and more points in this region so that we will, in any case, come very close to the ideal case. If necessary, we can treat the splitting off (115) even more accurately.

The low pressure increase long the trailing edge corresponds to a thinner profile. Therefore, we obtain the thinnest possible profile for a given problem.

In the case of the NACA examples, the shape of the profile, in particular its thickness, is specified by the problem and the calculation method. Large α_1 values, that is large c_a regions with pressure decrease intervals, and small φ_1, that is X_1 and large pressure decrease intervals, result in thick profiles and vice versa. In our method also, the profile is fixed uniquely by α_1, φ_1 and $\kappa_1(\eta)$, and the influence of α_1 and φ_1 remains the same. The calculation of the thinnest possible profile for a given problem means simultaneously that among the profiles with the same thickness and the same length of the pressure decrease intervals, the one calculated here has the greatest value α_1, and therefore the largest c_a interval with pressure decrease intervals.

The calculation of simple symmetric laminar profiles can be done in a complete manner using the present method.

b) Simple, asymmetric laminar profiles

Our formulas can immediately be expanded to the asymmetric case by modifying the assumptions a). In this way, this case can be completely treated just like the symmetric case. Again, we require only one region with constant velocity along the top side and the bottom side. Because of (122), (119), and (59), we select

$$\alpha_1 = \alpha_2 = \alpha_3 > \alpha_4 = \alpha_5 = \alpha_6. \tag{127}$$

Instead of (124), we make the following selection

$$\frac{1}{2}(\alpha_2 + \alpha_5) > 0. \tag{128}$$

where this variable was zero in the preceding case. For this, we will select φ_1 and φ_5, and because of (118) we now have available the beginning of the pressure increase along the top side and the bottom side. The functions $w_1(\varphi)$ and $w_5(\varphi)$ can be assumed, just like in a) (Figure 2).

According to (57) and together with (127), we find

$$\left.\begin{aligned} r_1 &= r_2 = r_3, \\ r_4 &= r_5 = r_6. \end{aligned}\right\} \tag{129}$$

The quantities φ_3, K_1, K_6, r_2 and v_5 are obtained from the calculation procedure. The velocity distributions obtained must be similar to those of a), but now the symmetry of $v^*(\varphi)$ at $\varphi = \pi$ is violated. Because of (128), the magnitude of the lift at $\alpha = \alpha_2$ is larger than at $\alpha = \alpha_5$, and, therefore, we must have /50

$$r_2 > r_5 \tag{130}$$

In a corresponding way, the velocity drop along the top side will be greater than along the bottom side, because the velocity $v(\varphi, \alpha)$ is continuous along the trailing edge because of (56). We obtain the variation of $v^*(\varphi)$ shown in Figure 6 (solid lines). Using (47) it is also possible to obtain the distributions $v(\varphi, \alpha_2)$ (solid lines) and $v(\varphi, \alpha_5)$ (dashed lines). If we transfer to X, we obtain approximately the distributions $v(X, \alpha_2)$ and $v(X, \alpha_5)$ of Figure 7, which again completely correspond to the requirement formulated in a) for the symmetric laminar profiles. For all angles of attack α between α_2 and α_5, the velocity increases from the nose along the top side up to X_1, and along the bottom side up to X_5.

Some information is already known on the shape of the profiles produced. A large value (128) leads to a high lift coefficient, and therefore, a greatly curved profile. The greatest

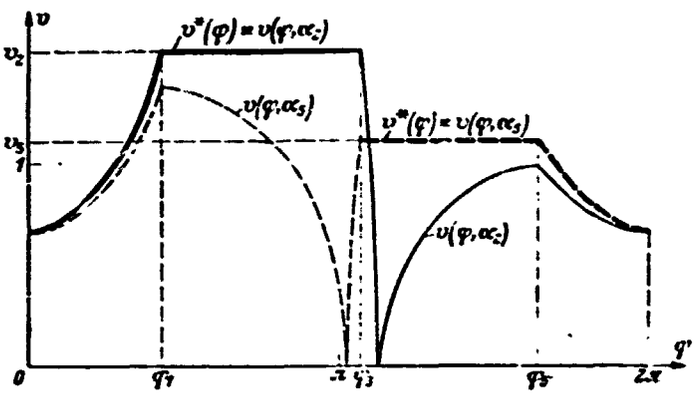

Figure 6. The functions $v^*(\varphi)$ and $v(\varphi,\alpha_5)$ for a simple asymmetric laminar profile (schematic).

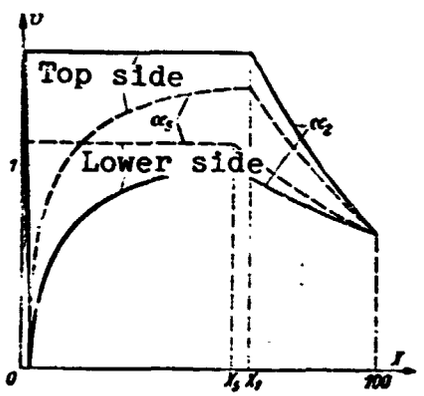

Figure 7. The functions $v(x,\alpha_5)$ for a simple asymmetric laminar profile (schematic).

α_2, which was important for the profile thickness in a), now corresponds to 1/2 of the difference of the angles of attack $1/2(\alpha_2 - \alpha_5)$, which together with (124) becomes α_2. If it is large, and if φ_1 and $2\pi - \varphi_5$ is small, then thick profiles are again produced, and vice versa. All of the calculated profiles are optimal in the same sense, just like for a).

Such asymmetric profiles have only been calculated approximately up to the present. According to a preceding paper [1], they could be calculated using conformal mapping. However, the surrounding of the profile nose brings about an unintentional drop in $v(\varphi,\alpha)$, especially for thick profiles, which again corresponds to the non-exploited tip of Figure 5. With the present method, this problem can be completely solved.

c) Double laminar profiles

The profiles calculated according to a) and b) have certain disadvantages. Their thickness depends uniquely on the problem. Profiles which have a large thickness always result in a large separation $\alpha_2 - \alpha_5$, which means a large c_a interval with laminar boundary layer. Now such a large region is often not necessary at all, for example for motor-driven airplanes, which fly at a single c_a under cruise conditions. If the simple laminar profiles of b) are used for this, then a relatively thin profile with a small $\alpha_2 - \alpha_5$ becomes a possibility. Except for the construction disadvantages of such profiles, large velocities rapidly appear at the nose for $\alpha > \alpha_2$, which do not make possible any high lift coefficients without flow separation. The other possibility would be a thick profile with a large $\alpha_2 - \alpha_5$. Such profiles, of course, are conditioned on high velocities at the edges and, of course, this introduces disadvantages. In addition, the α_2 values are not large enough so that favorable maximum lift values are achieved.

In order to avoid these disadvantages, we have introduced two regions of constant velocity each along the top side and the bottom side in our trial solution. We will explain the possibilities of profile design first of all with a symmetric example. By considering (124), we select

$$\alpha_3 > \alpha_2 = \alpha_1 > 0, \tag{131}$$

and corresponding to it, a φ_1 which, just like for a) will indicate the beginning of the pressure increase, as well as a φ_2 for which the X_2 according to (118) is close to the nose, say between $X_2 = 5$ and $X_2 = 10$. According to (118), φ_2 must lie /51

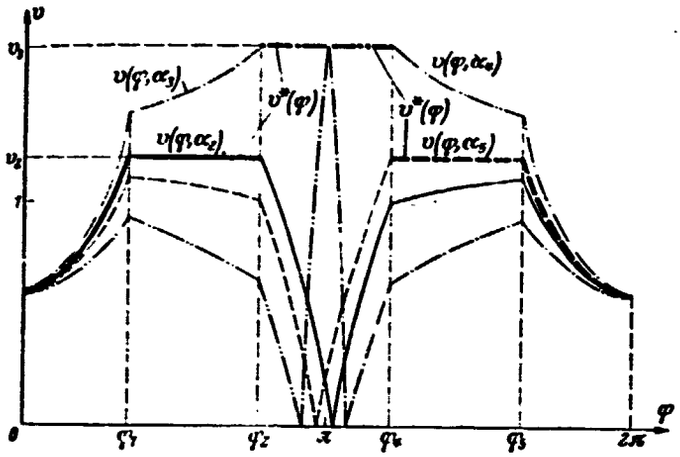

Figure 8. The functions $v^*(\varphi)$ and $v(\varphi,\alpha_i)$ for a double symmetric laminar profile (schematic).

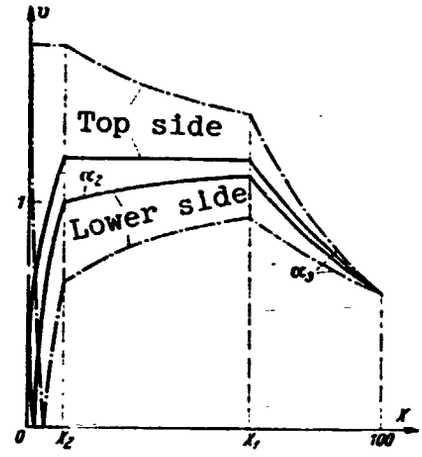

Figure 9. The functions $v(x,\alpha_i)$ for a double symmetric laminar profile (schematic).

approximately between 140° and 155°, therefore a considerable distance from π. The function $w_1(\varphi)$ will again be selected just like in a).

Because of (57), according to (131), we have

$$r_3 > r_2 = r_1, \tag{132}$$

and our method results in the approximate $v^*(\varphi)$ (solid line) shown in Figure 8, using approximately the same method as in a), and for which the distributions $v(\varphi,\alpha_i)$ can easily be determined using (47). The transition to X is shown in Figure 9. The lines for α_2 and α_5 as well as for α_3 and α_4 again coincide with exchanged top sides and bottom sides.

Such a profile now has two intervals with increasing velocity. For all angles of attack α with $\alpha_3 > \alpha > \alpha_4 = -\alpha_3$ the velocity along the top side and the bottom side increases up to X_2. For all angles of attack α with $\alpha_2 > \alpha \geq \alpha_5 = -\alpha_2$, it also

increases on both sides up to X_1. The second intervals are longer. They will primarily cause the laminar effects. It is now possible to make α_2 as small as required by the problem, without having to fear profiles which are too thin as well as their disadvantages. In order to avoid this, α_3 and φ_2 or X_2 are available. Using these variables, the profile thickness can be controlled using α_2 and X_1, just like for a). Large α_3 and X_2 result in thick profiles. In general, α_3 will be selected much larger than α_2 for the laminar profiles, so that usable profile thickness can be obtained with small X_2. The main advantage of the forward pressure decrease intervals is not the gain of the small laminar boundary layer interval. Instead, the maximum velocity, which occurs over the profile in the large α interval between α_3 and $-\alpha_3$, is given by the value v_3, which is relatively small, because it is assumed to exist over the entire profile interval (see the example in the next section). In all of the profiles calculated up to the present in comparably large α regions, we already have velocity peaks at the profile nose which are much greater. In this way, we obtain high lift without velocity peaks because of the fact that the velocity increases in the forward regions. This possibility always exists if the problem requires such small α_2 values, that is such small c_a regions with long pressure decrease intervals, so that profiles produced by it would be too thin in the case of the simple laminar profiles of a). These cases occur often. High maximum lift values are very important for landing and takeoff of motor-driven aircraft, where a small drag is necessary because a single value of c_a is used.

A sufficient decomposition of the nose suction tip occurs if the profile thickness is made greater by only a few percent (2 - 4%) due to the second laminar region compared with the corresponding simple laminar profile (with the same α_2). Therefore, we already obtain high lift coefficients with this slight thickness increase, and this results in only a small increase in the pressure along the back side and, therefore, a small increase /52 in the drag. The same thing can only be done with extremely large thickness (21%) with simple laminar profiles (see the example of Section 6).

On the other hand, if we compare simple and double laminar profiles of the same thickness and the same X_1, that is equal pressure drop and pressure increase intervals, then the double profile will have a smaller α_2 and therefore a smaller interval with a small drag. However, the value of the minimum drag is about the same. By giving up part of the α region with a small drag, we can obtain a high c_a and it is possible to combine the advantages of the thin and the thick profiles.

Such "double laminar profiles" can be calculated without any difficulty using our method, even for the asymmetric case. Instead of the high α_3, we have a large value $1/2(\alpha_3-\alpha_4)$. Instead of the small α_2, we have a small value $1/2(\alpha_2-\alpha_5)$. In this way, we only bring about an additional curvature of the profiles, and the velocities along the lower side become smaller than those along the top side. This is the same as what occurred during the transition from a) to b) with the simple laminar profiles. The maximum lift compared with the asymmetric profiles is also increased because of α_3. Using α_2 and α_5, it is possible to restrict the angle of attack range in which one wishes to produce low drag using long pressure decrease intervals and,

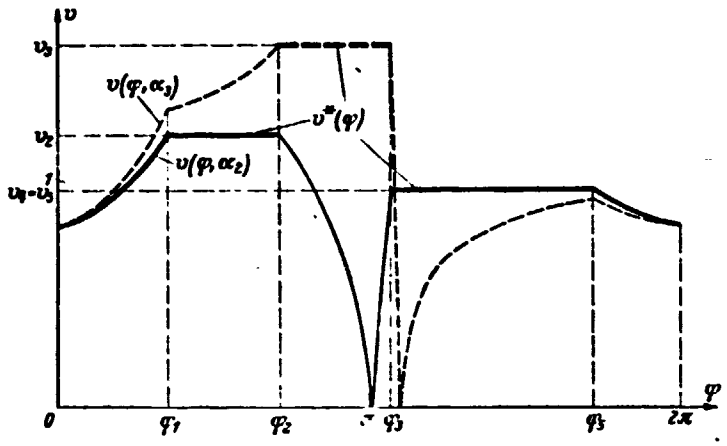

Figure 10. The functions $v^*(\varphi)$ and $v(\varphi,\alpha_i)$ for a special double asymmetric laminar profile (schematic).

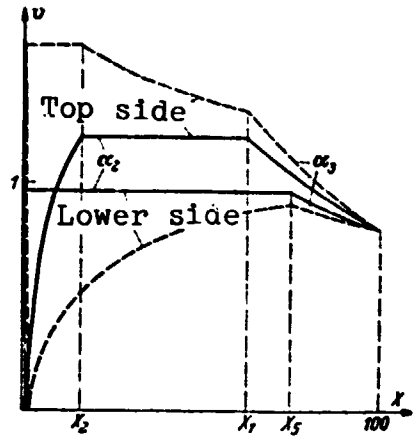

Figure 11. The functions $v(X,\alpha_i)$ for a special double asymmetric laminar profile (schematic).

therefore, long laminar boundary layers. α_3 and α_4 determines the limits of possible angles of attack which do not result in major flow separations.

For example, if only high angles of attack are permissible and if we are not interested in small angles of attack (diving flight), then we may select $\alpha_4 = \alpha_5$ and introduce the second laminar region on the top side only. By making the selection $\alpha_4 < \alpha_5$, the quantity $1/2(\alpha_3 - \alpha_4)$ and, therefore, the profile thickness is increased. Therefore, the effect along the top side can be increased by dropping this requirement, that is, by selecting α_3 or X_2 somewhat larger, so that again the same profile thickness is obtained. Our method is not restricted to any kind of symmetry.

A special profile of this type is produced if we, in addition to $\alpha_2 = \alpha_5$, require that

$$\alpha_3 > \alpha_1 = \alpha_2 = \alpha_4 = \alpha_5 = \alpha_6 \qquad (133)$$

For $\alpha_2 - \alpha_5 = 0$, we have a single angle of attack, for which a non-decreasing velocity occurs along the top side and the bottom side. Only with a large α_3 can we produce a high maximum lift. Just like in the preceding examples, we can obtain the distributions $v(\varphi, \alpha_i)$ and $v(X, \alpha_i)$ for this selection as shown in Figures 10 and 11.

Just like in Section 5a), in the case of the double laminar profiles we are interested in selecting the shapes $w_1(\varphi)$ and $w_6(\varphi)$ of the velocity decrease along the rear side, so that we again obtain $K_1, K_6 \approx 1$. In the symmetrical case, we can easily control this by means of α_3 or X_2 because these variables control the profile thickness which in turn is essentially responsible for the magnitude of the pressure increase along the back side. In the asymmetric case, it can happen that when $\frac{1}{2}(\alpha_3 - \alpha_4)$, X_2 and X_4 are specified, one of the two quantities K_1, K_6 remains much larger than 1, and the other remains much smaller than 1. In Section 5d) we will indicate how this can be equalized. /53

In general, a number of problems can be solved using the double laminar profile. The solution is always optimal in the sense mentioned above. The asymmetric profiles, which used to cause great difficulties, are automatically contained in the formulas.

An entire sequence of profiles can be calculated which have similar properties but different thicknesses, by for example, fixing $\alpha_i, \varphi_1, \varphi_5, w_1(\varphi)$ and $w_6(\varphi)$ and only changing φ_2 and (or) φ_4. Some computation effort is thereby spared for the repeated calculation of $F(\varphi)$. The transition to the profile must be carried out for each case, however.

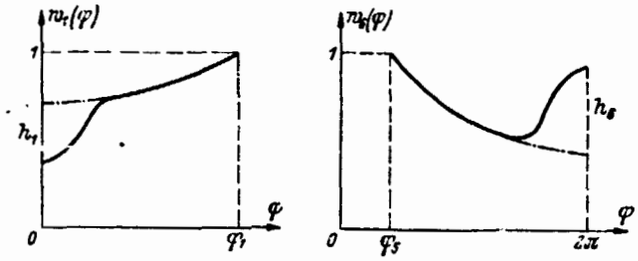

Figure 12. The selection of $w_1(\varphi)$ and $w_6(\varphi)$ for producing a high velocity difference up to the trailing edge.

d) The surrounding of the trailing edge

The velocity distribution in the vicinity of the trailing edge is determined by the functions $w_1(\varphi)$ and $w_6(\varphi)$, which up to the present have been assumed to approximately follow the variation shown in Figure 2. According to the preceding Figures 5, 7, 9, and 11, this makes the difference in the velocity $v(\varphi)$ between the top side and the bottom side decrease slowly to the value of zero toward the trailing edge.

In the case of the profiles calculated according to the approximation method, it has been found to be favorable to calculate back to the trailing edge using a non-zero velocity difference. This does not occur in reality, but the profiles calculated in this way had large velocity differences up to the vicinity of the trailing edge, and therefore produced a corresponding large amount of lift.

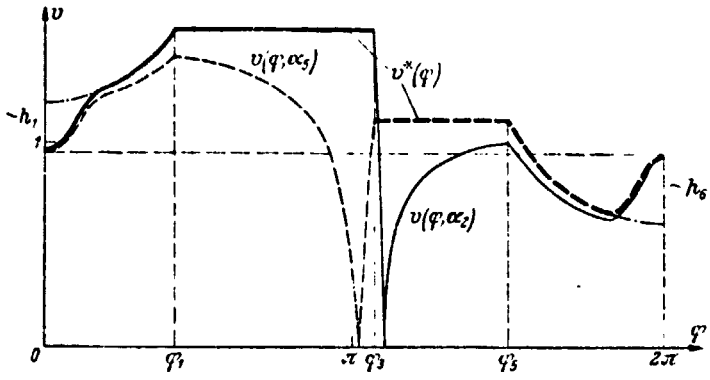

Figure 13. The consequences of h_1 and h_e for the variation of $v(\varphi)$ of a simple asymmetric laminar profile.

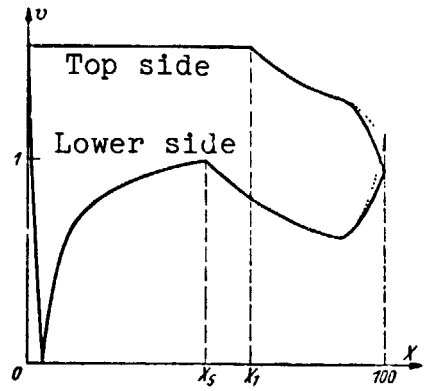

Figure 14. The consequences of h_1 and h_e in the variation of $v(X,\alpha_s)$ for a simple asymmetric laminar profile.

With our method, because of (56), it is not possible to specify any velocity jump at the trailing edge. However, just as happens in reality, we can hold the velocity difference between the top side and the bottom side fixed at a high value up to almost the trailing edge, and then let it suddenly and rapidly go to zero. This is successful if we select $w_1(\varphi)$ and $w_6(\varphi)$ according to Figure 12. We will introduce a rapid decrease in the quantity h_1 for $w_1(\varphi)$ in the vicinity of $\varphi = 0$. We will avoid a bend and select a continuous tangent. According to (121), it is to be horizontal at $\varphi = 0$. In a similar way, $w_6(\varphi)$ is given a rapid increase in the variable h_5 at $\varphi = 2\pi$. Therefore, for the example of a simple asymmetric laminar profile of b) (Figures 6 and 7), we find the functions $v(\varphi)$ and $v(X,\alpha_s)$ given in Figures 13 and 14, if we only change the functions $w_i(\varphi)$ compared with the previous case. Figure 14 exactly shows the intended high difference between the top side and the bottom side up to almost the trailing edge.

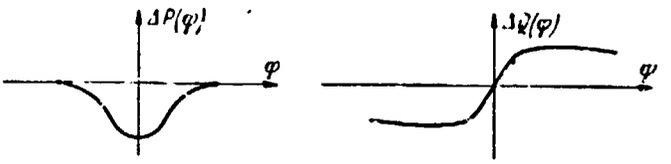

Figure 15. The changes $\Delta P(\varphi)$ and $\Delta Q(\varphi)$ when the velocity at the trailing edge is enlarged.

The quantity h_1 brings about a steep velocity decrease along the top side in the vicinity of the trailing edge. This is a pressure increase, which can easily lead to flow separation. On the other hand, h_6 produces a completely harmless pressure decrease. Therefore, one will attempt to make h_1 small and h_6 large (dotted line in Figure 14). Such a change results in approximately the change $\Delta P(\varphi)$ shown in Figure 15. According to /54 (34), the change $\Delta Q(\varphi)$ shown in Figure 15 also follows, which can easily be qualitatively verified. Therefore, according to (26), the inclination Θ becomes larger along the top side ($\varphi > 0$) and it becomes smaller along the bottom side ($\varphi < 0$). The profile produced becomes thinner along the trailing edge and more pointed. The limits of this additional slenderness is crossover.

This means that it is possible to reduce the pressure increase along the top side in the vicinity of the trailing edge by small h_1 and large h_6 and the profiles become thinner in the rear and more elongated. On the other hand, the reverse tendency can correct profiles which have a back side which is too thin (or which have a back side which crosses over).

The consequences of simultaneously enlarging or decreasing h_1 and h_6 can easily be seen. In the first case, we obtain (except for a rapid equalization of the velocity directly next

to the trailing edge, which according to experience does not have any serious disadvantages) the major velocity decrease along the bottom side (see Figure 14, for example). In the second case, we obtain it along the top side (see Figure 7). If all other variables remain the same, especially the remaining variation of $w_1(\eta)$ and $w_6(\eta)$, in the first case K_1 will decrease and K_6 will increase. The opposite will be true in the second case. We can vary these arbitrarily without any difficulty.

Our method is applicable for a number of important problems. We will now give a numerical example to gain explain the details.

6. Example

We will verify our method without dealing with a simplified special case, using the example of an asymmetric double laminar profile, which comes from the area of glider wings. In this case, an extremely low drag is required in the c_a range between $c_a = 0.4$ and 0.6. At the same time, large lift coefficients without any substantial flow separation are required. We will assume $2N = 60$ and select

$$\begin{aligned} \alpha_1 = \alpha_2 &= -4.95^\circ, & \varphi_1 = \tau_7 &= 42^\circ, \\ \alpha_3 &= 13.20^\circ, & \varphi_2 = \tau_{27} &= 162^\circ, \\ \alpha_4 = \alpha_5 = \alpha_6 &= 3.30^\circ, & \varphi_4 = \varphi_5 = \tau_{47} &= 282^\circ. \end{aligned}$$

The range between α_5 and α_2 corresponds to the c_a range between 0.4 and 0.6, according to (100). In this range, the velocity along the top side increases up to X_1, for which according to (118) we have $X_1 \approx 90$. On the bottom side this is true up to $X_5 \approx 60$. This means that we will obtain large laminar effects in this range. The c_a values below 0.4 are of no interest, but those above 0.6 are important. Therefore, we will assume

$\alpha_4 = \alpha_5$ and not introduce the decomposition of the suction tip below α_5. We will consider the high c_a values with a large α_3 value only. For this case, the velocity along the top side decreases already starting at $X_2 \approx 5$. The boundary layer becomes turbulent soon and already has a large thickness in the vicinity of the trailing edge. In order to not produce substantial separations, we have selected X_1 greater than X_5 and have displaced the main velocity drop, which of course must exist for closure of the profile, along the bottom side. On the top side, we introduce

$$\kappa_1(\varphi) = 1 - h_1\left(\frac{\cos\varphi - \cos\varphi_1}{1 - \cos\varphi_1}\right)^2, \tag{134}$$

$h_1 = 0.36$, which is a short pressure increase which is required for the pressure equalization along the trailing edge according to Section 5d). We select the following form of the pressure increase along the bottom side

$$\left.\kappa_6(\varphi) = \left(1 + \kappa_6 \frac{\cos\varphi - \cos\varphi_5}{1 - \cos\varphi_5}\right)^{-0.22} \{\{\}\}^{-1}\right\} \tag{135}$$

where

$$\{\{\}\} = 1 \text{ for } \varphi < \varphi_5^*$$

and $\kappa_6 = 1.266$, $h_6 = 0.2025$, $\varphi_5^* = \tau_{55} = 330°$. The first term is approximately the velocity decrease, as recommended by F. X. Wortmann [10]. The second term in (135) gives the contribution on the bottom side towards the pressure equalization at the trailing edge. It was selected relatively small with a relatively small h_6 value. Correspondingly, the contribution of the top side towards the pressure equalization is larger, which according to Section 5d) results in a complete trailing edge. The pressure equalization terms were introduced as multiplication factors because of the calculation, so that the meaning of the quantities /55

h_1 and h_6 is somewhat modified compared with their meaning in Figure 12.

The calculation procedure is now given by Section 4. The W_{ci}, W_{si} of (61) and (62) can be evaluated in closed form. We obtain

$$\int_0^{\psi} \cos\varphi \ln\left(1 - m\frac{\cos\varphi - \cos\psi}{1-\cos\psi}\right) d\varphi = \int_{2\pi-\psi}^{2\pi} \cos\varphi \ln\left(1 - m\frac{\cos\varphi - \cos\psi}{1-\cos\psi}\right) d\varphi = -\lambda\psi - \sin\psi + 2\sqrt{\lambda^2-1}\arctan\left(\frac{\sqrt{\lambda^2-1}}{\lambda-1}\tan\frac{\psi}{2}\right). \tag{136}$$

$$\lambda = \frac{1}{m} - \left(\frac{1}{m} - 1\right)\cos\psi.$$

For negative m, we have $\lambda < 1$, so that for the last term we must transfer to $\mathfrak{Re}\mathfrak{g}$, as is known. In addition, we have

$$\int_0^{\psi} \sin\varphi \ln\left(1 - m\frac{\cos\varphi - \cos\psi}{1-\cos\psi}\right) d\varphi = -\int_{2\pi-\psi}^{2\pi} \sin\varphi \ln\left(1 - m\frac{\cos\varphi - \cos\psi}{1-\cos\psi}\right) d\varphi = -(1-\cos\psi)\left[1 + \left(\frac{1}{m} - 1\right)\ln(1-m)\right]. \tag{137}$$

Therefore, according to (61) and (62), if we introduce the φ_i and φ_i^* for ψ, the h_i and $\varkappa_i$ for m,

$$W_{c1} = 0.157262, \quad W_{s1} = -0.034880, \quad \ln \varkappa_1(0) = -0.446287,$$
$$W_{c6} = 0.427715, \quad W_{s6} = -0.305324, \quad \ln \varkappa_6(2\pi) = -0.350185$$

and according to (79) to (81),

$$D_1 = 0.124948, \quad D_2 = -0.245954, \quad D_3 = -0.062935.$$

In the transcendental equation (82), we have

$$a = 0.242120, \quad b = -0.801684, \quad c = 0.951164, \quad d = 0.034488,$$

from which we find

$$\varphi_3 = 193^\circ\,58'\,48'' = 3.385590$$

This value is determined very accurately. Accordingly (88)

$$J_4 - \pi = -0.544720, \qquad J_5 = 0.256317, \qquad J_6 = -0.071977$$

and according to (83) and (84)

$$K_1 = 0.90074, \qquad K_6 = 0.94239.$$

The pressure increase in (135) and the profile thickness which is essentially determined by it is found to be sufficiently large, so that for our small value $\frac{1}{2}(d_2 - d_3) = 0.825^\circ$ there is still enough play for the forward laminar interval. Using the indicated values for φ_2 and α_3, we achieve $K_6 \approx 1$ exactly. This was not found immediately, but since the influence of φ_2 on K_6 is easily seen (small φ_2 results in a larger profile thickness and larger K_6), it was easy to specify φ_2.

Now we will calculate the $\bar{P}$, according to (90), v_1 according to (98), $r^*(\eta)$ according to (52), and possibly a few $r(\varphi, d_i)$ according to (47). We will test whether there are small effects caused by the v_i and the K_i. We do not have to give the tabulated values of these calculations, because the results give everything important. The transition (94) to the ζ, as well as the calculation of the $\dot{x}, \dot{y}$, poses no difficulties. In (101) and (102) we will use $\beta = 8^\circ$. This value can easily be selected because of the profile inclination angle $\Theta(\eta)$ already contained in the $\dot{x}$, and $\dot{y}$, so that the profile in the X, Y system has approximately the usual position. The error ε_x and ε_y are the following according to (107):

$$\varepsilon_x = -0.00082, \qquad \varepsilon_y = -0.00149,$$

ε i are therefore sufficiently small for a length of $l_1 \approx 0.9$. /56
After equalizing them and making the transition to X and Y, we find the profile coordinates given in Table 3 as well the values of

$$\frac{1}{l_1} = \frac{1}{2\pi} \cdot \frac{dc_a}{dx} \qquad (138)$$

according to (100). We also obtain the values of c_{m0} according to (42) and (43). The value of c_{m0} indicates a relatively high nose-heavy moment. This disadvantage does not play any role because of the slender wings of gliders, compared with the other advantages. The longitudinal stability can also easily be brought about and the rotational thickness of the laminar wings is also sufficient, because they are usually built out of whole shells because of the high surface quality.

Figure 16 shows the distributions $v(X, \alpha_i)$ for the three α_i values which are required for calculating the boundary layer. The lines $v^*(\varphi)$ are darkened. In addition, we show the calculated profile.

The example gives one an idea of the possibilities of design for the double laminar profile. Up to $\alpha = \alpha_3 = 13.2°$, which corresponds to $c_a \approx 1.6$ because of (100), the maximum velocity is $v_{max} = 1.98$. The profile thickness remains so small that between α_2 and α_5, between $c_a = 0.5$ and $c_a = 0.6$ because of (100), and along the top side up to $X_1 = 90$, along the bottom side up to $X_5 = 50$, there are pressure decreases. The value of X_5 produced is somewhat displaced compared with (118). The displacement is present for all curved profiles along the bottom side to a certain extent, and could have been predicted based on similar examples. At the trailing edge, the pressure increase along the top side is much greater than the decrease along the bottom side. In this way, we obtain almost exactly a finite trailing edge angle (Figure 16), even though it vanishes

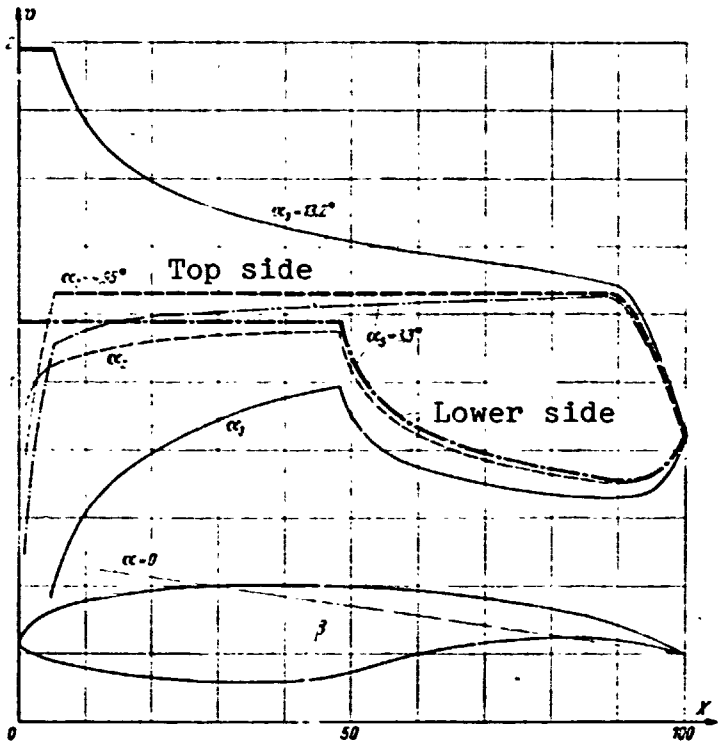

Figure 16. The profile for the sample calculation with its distributions $v(x, \alpha_i)$.

TABLE 3*

THE COORDINATES OF THE PROFILE CALCULATED AS AN EXAMPLE

X	Y	X	Y	X	Y
100,00	0,00	29,51	10,02	17,49	—3,27
99,67	0,13	25,06	9,77	21,44	—3,66
98,73	0,53	20,87	9,13	25,64	—3,97
97,29	1,20	16,98	9,00	30,01	—4,15
95,15	2,08	13,43	8,18	34,58	—4,21
93,28	3,05	10,26	7,87	39,20	—4,10
90,78	4,02	7,52	7,19	43,84	—3,80
87,92	4,92	5,24	6,42	48,37	—3,12
81,67	5,75	3,42	5,50	53,19	—1,79
81,05	6,53	1,97	4,48	58,65	—0,34
77,09	7,25	0,90	3,45	64,40	0,82
72,84	7,91	0,23	2,47	70,18	1,71
68,35	8,49	0,01	1,65	75,82	2,27
63,66	9,01	0,41	0,97	81,16	2,53
58,82	9,44	1,43	0,31	86,06	2,18
53,88	9,78	2,99	—0,35	90,39	2,17
48,89	10,02	5,05	—1,01	94,00	1,63
43,91	10,17	7,57	—1,64	96,74	0,99
38,98	10,22	10,50	—2,24	98,60	0,45
34,17	10,17	13,82	—2,79	99,66	0,11
				100,00	0,00

$\frac{1}{l_1} = 1{,}1097 \qquad c_{m0} = -0{,}2097$

* Translator's Note: Commas indicate decimal points.

mathematically. It would be possible to make h_1 somewhat smaller and h_6 larger, and to save the pressure increase along the top side. However, not much can be done here, because the trailing edge which becomes more slender according to Section 5d) rapidly reaches the limit of crossover. Even the example shown has a very full trailing edge. A similar calculation showed a small crossover without being able to reduce the pressure increase along the top side. The lift increase in the vicinity of the trailing edge, according to Section 5d), always brings about a /57 pressure increase along the top side according to potential theory, which is reduced by boundary layer and separation influences. This has been found not to be a disadvantage in the approximately calculated profiles *. It is possible that, in other example calculations, it will be possible to select a larger h_1 and a smaller h_5, so that, depending on the requirements, we can obtain trailing edges which are not as slender.

The details of the velocity distribution can also be fine-tuned just like its variation along the trailing edge. This is the topic of other example calculations which goes beyond the scope of this basic method.

7. Summary

Simple formulas are derived for direct termination of the wing profile from its velocity distribution, which at the same time makes it possible to determine whether a specificed velocity distribution corresponds to a closed profile which is reasonable. Because the formulas are simple, a special trial solution for the velocity distribution can be used, which is based on an

*See, for example NACA report 824, Footnote on page 15.

important generalization of the laminar profiles known up to the present. The computation method is built up including numerical details and is verified with one example.

REFERENCES

1. Eppler, R. Ing. Archiv., Vol. 23, 1955, p. 436.

2. Lighthill, M. J. A New Method of Two-Dimensional Aerodynamic Design, Aeron. Res. Council, Rep. and Mem., No. 2112, London, 1945.

3. Hurwitz, A. and R. Courant. Funktionentheorie (Function Theory), 2nd Edition, Berlin, 1925.

4. Garrick, I. E. Conformal Mapping in Aerodynamics, with Emphasis on the Method of Successive Conjugates. Proceedings of a Symposium: Construction and Application of Conformal Maps, Washington, 1952.

5. Weinberger, W. Luftfahrtforschung, Vol. 17, 1940, p. 3.

6. Glauert, H. Die Grundlagen der Tragflügel- und Luftschraubentheorie (Basics of Airfoil and Airscrew Theory), Berlin, 1929.

7. Mangoldt, H. v. and K. Knopp. Einfuhrüng in die höhere Mathematik (Introduction to Higher Mathematics), Vol. 3, Leipzig, 1944, p. 508.

8. Runge, C. and H. Konig, Vorlesungen über numerisches Rechnen (Lectures on Numerical Calculations), Berlin, 1924.

9. NACA Report No. 824, footnote p. 15.

10. Wortmann, F. X. Z. Flugwiss, Vol. 3, 1955, p. 333.

Translated for National Aeronautics and Space Administration under Contract No. NASw-2483 by SCITRAN, P. O. Box 5456, Santa Barbara, California, 93108.

STANDARD TITLE PAGE

1. Report No. NASA TT F-15,417	2. Government Accession No.	3. Recipient's Catalog No.
4. Title and Subtitle DIRECT CALCULATION OF AIRFOILS FROM PRESSURE DISTRIBUTION		5. Report Date March 28, 1974 6. Performing Organization Code
7. Author(s) R. Eppler		8. Performing Organization Report No. 10. Work Unit No.
9. Performing Organization Name and Address SCITRAN Box 5456 Santa Barbara, CA 93108		11. Contract or Grant No. NASw-2483 13. Type of Report and Period Covered Translation
12. Sponsoring Agency Name and Address National Aeronautics and Space Administration Washington, D.C. 20546		14. Sponsoring Agency Code

15. Supplementary Notes

Translation of "Direkte Berrechnung von Tragflugelprofilen aus der Druckverteilung," Ingenieur-Archive, Vol. 25, No. 1, 1957, pp. 32-57.

16. Abstract

Supplementing author's paper indexed in Engineering Index 1956, p. 56, from Vol. 23, No. 6, 1955 issue, improved calculating method is described, employing simple formulas.

17. Key Words (Selected by Author(s))	18. Distribution Statement
	Unclassified - Unlimited

19. Security Classif. (of this report)	20. Security Classif. (of this page)	21. No. of Pages	22. Price
Unclassified	Unclassified	62	